Biogeosciences, 22, 5283–5308, 2025
https://doi.org/10.5194/bg-22-5283-2025

Biogeosciences Open Access EGU

Research article

Ecosystem dynamics of an ice-poor permafrost peatland in eastern Eurasia: paleoecological insights into climate sensitivity

Zhengyu Xia[1,★], **Fengtong Chen**[1,★], **Mengyang Guo**[1], **and Zicheng Yu**[1,2]

[1]Key Laboratory of Geographical Processes and Ecological Security in Changbai Mountains, Ministry of Education, School of Geographical Sciences, Northeast Normal University, Changchun, 130024, China
[2]State Key Laboratory of Black Soils Conservation and Utilization, Northeast Institute of Geography and Agroecology, Chinese Academy of Sciences, Changchun, 130102, China
[★]These authors contributed equally to this work.

Correspondence: Zhengyu Xia (zhyxia@hotmail.com) and Zicheng Yu (yuzc315@nenu.edu.cn)

Received: 27 February 2025 – Discussion started: 12 March 2025
Revised: 16 July 2025 – Accepted: 25 July 2025 – Published: 6 October 2025

Abstract. Northern peatlands are carbon-rich ecosystems highly sensitive to climate change, with nearly half of their carbon stocks associated with permafrost. Peat-based paleoecological records provide insights into the complex responses of permafrost peatlands to long-term climate variability, but most studies have been conducted in ice-rich permafrost peatlands in Europe and North America. Here, we use multiple active-layer cores to reconstruct the ecosystem history of an ice-poor permafrost peatland in eastern Eurasia, near the southernmost limit of circum-Arctic permafrost but outside the distribution of circum-Arctic thermokarst landscape.

Our results show that the peatland, which has developed on a floodplain since the late Holocene cooling, underwent a major phase of lateral expansion during the Little Ice Age. A fen-to-bog transition occurred in recent decades, with dry-adapted *Sphagnum* mosses replacing herbaceous vegetation across the site and having rapid surficial peat accumulation. Carbon isotope ratios of *Sphagnum* macrofossils, a proxy for surface wetness, indicate that *Sphagnum* mosses were initially established under very dry conditions but that their habitats have since become gradually wetter.

Synthesizing these findings, we highlight that (1) permafrost aggradation during climate cooling may promote new peatland formation over permeable mineral substrate by impeding drainage; (2) anthropogenic climate warming and active-layer deepening can induce an ecosystem-scale regime shift, but ice-poor permafrost peatlands generally exhibit stability and homogeneity due to the absence of dynamic surface morphology (such as frost heave and thermokarst collapse); (3) ongoing wetting may result from surface adjustment–hydrology feedback and vegetation–hydrology feedback, demonstrating the internally driven resilience of ice-poor permafrost peatlands in maintaining their hydrology and carbon accumulation; and (4) ice-poor permafrost peatlands are likely to remain persistent carbon sinks under ongoing and future climate change.

1 Introduction

Northern peatlands are globally important and persistent carbon (C) sinks over time (Gorham, 1991; Yu et al., 2011; Treat et al., 2019), with the size of their C stocks estimated to be 400–500 Pg C (Yu, 2012; Hugelius et al., 2020). Almost half of the northern peatland C is affected by circum-Arctic permafrost (Smith et al., 2007; Hugelius et al., 2020). This biosphere–cryosphere interaction renders permafrost peatlands – commonly found in northern high latitudes – highly sensitive to climate warming and permafrost degradation, which, beyond the simple thawing process, entails compound changes in surface morphology, hydrology, soil structure, vegetation composition, and erosion regime (Payette et al., 2004; O'Donnell et al., 2012; Borge et al., 2017; Olefeldt et al., 2021; Errington et al., 2024). There is a growing concern that degradation of C-rich permafrost peatlands may trigger strong C-cycle feedback that will further accelerate climate warming in the future (Schneider von Deimling et al., 2012; Turetsky et al., 2020).

Permafrost peatlands are heterogeneous landscape features dominated by diverse landforms across permafrost zones (Zoltai and Tarnocai, 1975; Vitt et al., 1994). For example, perennial frost mounds such as palsas or peat plateaus are found in the boreal zone, whereas ice-wedge polygons are found in the Arctic tundra zone (Treat et al., 2016; Olefeldt et al., 2021). These landforms are not always in equilibrium with the climate (Camill and Clark, 1998; Vitt et al., 2000) and may undergo multiple and locally inconsistent stages of transition in response to permafrost degradation (Swindles et al., 2015; Hugelius et al., 2020; Olefeldt et al., 2021), forming new lakes, ponds, fens, and bogs. Generally, field-based greenhouse gas flux measurements and laboratory-based incubation or mesocosm experiments indicate that decomposition of previously frozen organic matter (OM), once upon thaw, has the potential to increase emissions of both CO_2 and CH_4 (and N_2O) (Turetsky et al., 2002; Hodgkins et al., 2014; Voigt et al., 2017, 2019). Direct measurements of belowground C stocks across a chronosequence also present evidence for possibly substantial losses of organic C following thaw and surface collapse (O'Donnell et al., 2012; Jones et al., 2017; Harris et al., 2023). However, these studies yield highly diverse results due to methodological biases, regional variations (permafrost history and peat type), and local processes (geomorphic setting and hydrology) (Treat et al., 2014; Cooper et al., 2017; Estop-Aragonés et al., 2018; Knoblauch et al., 2018; Heffernan et al., 2020; Manies et al., 2021; Heffernan et al., 2024). Therefore, predicting the future fate and trajectory of C stored in permafrost peatlands as well as their climate feedback relies on empirical equilibrium models due to spatiotemporal complexities inherent to such systems (Hugelius et al., 2020; Turetsky et al., 2020; Treat et al., 2021; Fewster et al., 2022).

Paleoecological records derived from peatland archives offer crucial insights into how permafrost peatlands respond to climate variability during their own development histories and are particularly relevant to understanding the slow changes in and interactions among climate, permafrost, hydrology, vegetation, disturbance, and C accumulation on decadal to millennial timescales (Camill et al., 2009; Bauer and Vitt, 2011; Hunt et al., 2013; Jones et al., 2013; Swindles et al., 2015; Gałka et al., 2017; Xia et al., 2024a). Among boreal peatlands, multiple records document that permafrost aggradation during Holocene climate cooling resulted in elevated and drier peatland surfaces, with an increased abundance of bog-like vegetation (shrubs and *Sphagnum* mosses), more frequent and severe wildfires, and decreased C accumulation rates (Robinson and Moore, 2000; Oksanen et al., 2001; Turetsky et al., 2007; Hunt et al., 2013; Treat et al., 2016). During the current warm period with permafrost thaw, high-resolution proxy records, however, show diverse ongoing ecohydrological trajectories, with some shifting drier due to deeper active layers or higher evapotranspiration rates, some shifting wetter due to accelerated thaw or surface collapse, and some experiencing fluctuating conditions (Zhang et al., 2022). These diverse trajectories have had different impacts on peatland C accumulation rates (Swindles et al., 2015; Zhang et al., 2018a; Sim et al., 2021). Moreover, there is growing evidence of vegetation shift in recently drying permafrost peatlands toward the dominance of *Sphagnum* mosses (Magnan et al., 2018; Taylor et al., 2019; Chartrand et al., 2023; Piilo et al., 2023; Cleary et al., 2024), a well-known "peat builder" that may enhance the C sink capacity through multiple mechanisms (Clymo and Hayward, 1982; van Breemen, 1995).

Despite the progress to date, it is noteworthy that the current literature and relevant knowledge about the histories and present states of permafrost peatlands are disproportionately built on studies carried out across ice-rich permafrost environments in Europe and North America. Conversely, there are very few counterpart records documented from eastern Eurasia (Treat et al., 2016), which encompasses a vast area and a further southward, inland distribution of circum-Arctic permafrost (Fig. 1a). Therefore, our understanding of the processes and mechanisms governing the response of permafrost peatlands to climate change may be incomplete.

Northern Northeast China is situated at the southernmost limit of circum-Arctic permafrost (Fig. 1b). Regional permafrost degradation caused by climate warming and human activities has been widely documented over recent decades (Jin et al., 2000). Although peatlands are abundant in this region (Xing et al., 2015), only a limited number of sites have been thoroughly described and investigated so far. These studies have mostly focused on greenhouse gas fluxes (Miao et al., 2012a; Yu et al., 2017; Sun et al., 2024), biogeochemical cycling (Wang et al., 2010; Guo et al., 2018; Ramm et al., 2022), and C accumulation patterns (Xing et al., 2015; Liu et al., 2019a) or use peatlands as archives for reconstructing past wildfire, dust, pollution, and upland forest histories (Bao et al., 2012, 2014; Gao et al., 2018; Liu et al., 2025). Only a few studies have aimed to explicitly examine their long-term ecosystem histories using peat-core analysis (Liu et al., 2024b; Xia et al., 2024a). Furthermore, despite the presence of permafrost, this region is not within the modern distribution of circum-Arctic thermokarst landscape (Fig. 1a) due to the underlying ice-poor conditions (Brown et al., 1997; Jin et al., 2016; Olefeldt et al., 2016). Regional peatlands barely show ground expansion- or collapse-related surface terrain characteristics, unlike those ice-rich European and North American permafrost peatlands extensively described in the literature (Olefeldt et al., 2021). Therefore, it remains unclear whether and how climate–permafrost dynamics affect regional peatlands or whether such dynamics differ from other permafrost regions.

Herein, we aim to address these critical data and knowledge gaps by analyzing peat properties, plant macrofossils, and moisture indicators from six radiocarbon-dated active-layer cores to reconstruct the ecosystem history of a bo-

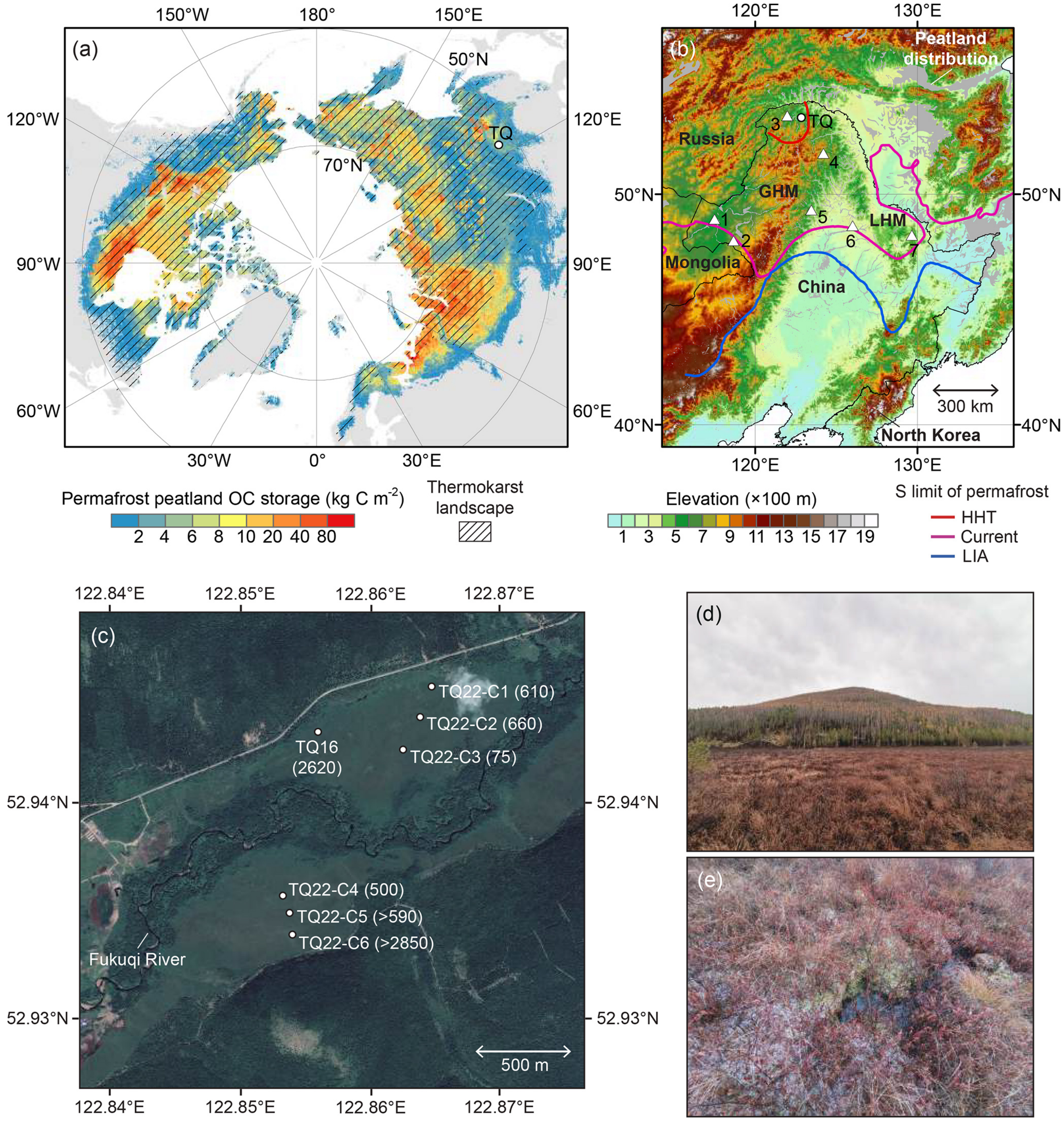

Figure 1. Overview of the study region and site. **(a)** Circum-Arctic map of permafrost peatland organic carbon (OC) storage from Hugelius et al. (2020), overlain by the thermokarst landscape distribution from Olefeldt et al. (2016) in hatched areas and the location of Tuqiang (TQ) peatland – our study site. **(b)** Map of Northeast China showing absolute elevation (a.s.l.), the distribution of peatlands or peat-forming wetlands (Xu et al., 2018), the location of Tuqiang peatland, the location of other paleoclimate records later mentioned in this paper (1: Hulun Lake; 2: Yihesariwusu Lake; 3: Huola Basin; 4: Hongtu Peatland; 5: Sifangshan Lake; 6: Tianchi Crater Lake; 7: Tanghongling Mire), the current southern limit of permafrost (Brown et al., 1997), and the inferred southern limits of permafrost during the Holocene Hypsithermal period (HHT) and the Little Ice Age (LIA) in China (redrawn from Jin et al., 2000). GHM: Greater Hinggan Mountains; LHM: Lesser Hinggan Mountains. **(c)** Google Earth aerial image (© Google Earth 2025, CNES/Airbus) of Tuqiang peatland, showing the locations of cores collected in this study (TQ22) and a previous study (TQ16) by Han et al. (2019). The numbers in parentheses indicate peat initiation ages in cal. yr BP. TQ22-C5 and TQ22-C6 did not reach the basal peat; thus peat initiation ages should be earlier than their oldest ages. **(d)** Field view of Tuqiang peatland (in front of a hill). **(e)** Close-up view of Tuqiang peatland vegetation (with whitish snowflakes at the time of field sampling in September 2022). A description of the taxa can be found in Sect. 2.1.

real ice-poor peatland in permafrost-affected northern Northeast China. Specifically, our objectives are to (1) determine how peatland formation and development, including long-term changes in ecosystem structure and function, responded to past climate variability and (2) understand the role of permafrost in regulating these changes. These objectives are driven by our overarching hypothesis that climate–permafrost interactions and relevant feedback are fundamental in shaping the long-term evolution of peatlands, but due to the absence of dynamic surface morphology (such as frost heave and thermokarst collapse) in ice-poor permafrost environments, the specific processes and mechanisms are expected to differ from those in ice-rich permafrost peatlands. Collecting multiple cores allows us to draw a comprehensive picture of peatland history, capture the spatial heterogeneity of surface features and/or ground properties, and reduce biases that can arise from relying on a single core.

2 Materials and methods

2.1 Study site and sampling

Our study site is Tuqiang peatland (52.94° N, 122.86° E; elevation 475 m a.s.l.) in the northern Greater Hinggan Mountains of Northeast China, near the border with Russia (Fig. 1b). From nearby Mohe weather station (1959–2022), the mean annual temperature is −4.1 °C with above-zero temperatures occurring from May to September. The mean annual precipitation is 443 mm, of which 365 mm falls between May and September. This site is within the "predominantly continuous permafrost" zone based on a national classification, which has been considered more regionally suitable (Ran et al., 2012; Zhang et al., 2021). It differs from the "discontinuous permafrost" zone provided by the International Permafrost Association (Brown et al., 1997) and "sporadic permafrost" zone based on the equilibrium state model (Obu et al., 2019). The permafrost coverage is 65 %–75 %, and the mean active-layer thickness is about 1 m (Ran et al., 2012; Wen et al., 2021). The mean annual ground temperature is about −2 °C at 1.5–2.5 m depth based on the borehole measurements taken nearest to the study site (Li et al., 2022). The soil is dominated by ice-poor frozen soil and ice soil (Fan et al., 2023; Zhang et al., 2023), with ground ice mainly found in the 30 m below the ground surface (Zhang et al., 2024).

Tuqiang peatland developed on a floodplain as part of a larger peatland complex extending along the Fukuqi River (Fig. 1c). Peatland vegetation varies with microform features across the site, with hummocks dominated by *Sphagnum* mosses (such as nutrient-poor species *S. magellanicum* and *S. capillifolium*) and Ericaceae shrubs (*Vaccinium uliginosum*, *Rhododendron tomentosum*, and *Chamaedaphne calyculata*) and hollows dominated by tussock sedges (*Eriophorum vaginatum*) (Fig. 1e; Miao et al., 2012a; Liu et al., 2024b; Sun et al., 2024). Other notable plant species include *Alnus hirsuta*, *Betula fruticosa*, *Salix rosmarinifolia*, *Calamagrostis angustifolia*, *Carex* spp., and *Polytrichum* spp. The peatland hydrology is mainly controlled by precipitation and evapotranspiration fluxes, as well as seasonally changing thaw depth, without obvious influence from nutrient-rich surface water and groundwater inflows (Liu et al., 2024b; Sun et al., 2024). The maximum thaw depth is 50–70 cm, which occurs in October (Wang et al., 2023; Sun et al., 2024). The water table depth generally varies between 10 and 35 cm below shrub–moss hummocks during the growing season, reaching its peak depth in mid-summer if there is no heavy-precipitation event, based on previous field monitoring data (Miao et al., 2012a; Liu et al., 2024a).

Tuqiang peatland has not developed any outstanding permafrost-related surface terrain features such as palsas, peat plateaus, thermokarst collapses, or ponds (Fig. 1d). As a nationally well known site, it has been studied for over a decade with an eddy covariance tower monitoring greenhouse gas fluxes in the northern section (Yu et al., 2017; Sun et al., 2024).

In September 2022, we collected six active-layer cores from *Sphagnum*-dominated surfaces in Tuqiang peatland using a stainless-steel serrated knife and a 7 × 7 cm box corer: three from the northern section and three from the southern section (Fig. 1c). Their key information is summarized in Table 1. Briefly, two cores, TQ22-C5 and TQ22-C6, did not reach basal peat and mineral substrate. All cores were stored in the laboratory under frozen conditions.

2.2 Laboratory analysis

The collected peatland cores were cut with a band saw in the laboratory into 1 cm slices, which were subsequently subsampled for all the analyses. Due to complications during transportation from the field to the laboratory, some core sections experienced compression or expansion by a few centimeters compared to the original core lengths measured in the field. Assuming that compression or expansion was uniform across the cores, sample depths were corrected if necessary to match the field-measured core lengths (Table 1).

Physical properties of cores were analyzed at 1 cm intervals following the standard protocol of loss on ignition (Chambers et al., 2010). Briefly, subsamples of 1 cm^3 were dried in an oven at 105 °C for 24 h to measure water content and dry bulk density. Then, the dried subsamples were burned in a muffle furnace at 550 °C for 4 h to estimate OM content and ash-free bulk density (AFBD). Bulk peat concentrations of the C and nitrogen (N) of cores were analyzed at 2 cm intervals for peat sections. Additional subsamples were oven-dried, and 1.5–2 mg of the dried material was ground using a ball mill and weighed into tin capsules. Measurements were carried out with an elemental analyzer (EA3000, EuroVector, Italy). The analytical precision (1σ) was about 0.4 % for C and 0.2 % for N concentrations.

Table 1. Key information about collected peat cores from Tuqiang peatland.

Core ID	Latitude (° N)	Longitude (° E)	Core length[a] (cm)	Peat section depth (cm)	*Sphagnum* peat section depth (cm)
TQ22-C1	52.9453	122.8647	57	0–49	0–16
TQ22-C2	52.9440	122.8639	52	0–34	0–23
TQ22-C3	52.9425	122.8628	81	0–43	0–38.9[b]
TQ22-C4	52.9340	122.8540	69	0–59.3[b]	0–45.7[b]
TQ22-C5	52.9349	122.8537	60	0–60	0–30
TQ22-C6	52.9357	122.8533	65	0–65	0–26, 30–41[c]

[a] Measured in the field. [b] Decimals are reported to correct core compression or expansion during sample transportation. [c] Gap in *Sphagnum* peat section is due to changes in macrofossil compositions.

All cores were analyzed for ^{14}C dates at a few selected horizons. They have one date at the depth contiguous to the basal peat or the bottom of the available peat (a few centimeters above for TQ22-C1 due to the general lack of credible macrofossil materials), which we refer to as "basal ages" or "oldest ages". All cores also have one date close to the depth interpreted as the onset of *Sphagnum* peat over sedge peat. *Sphagnum* moss fragments or the aboveground part of vascular plant fragments from 1 cm^3 subsamples were separated and concentrated under a stereomicroscope as dating materials and then were freeze-dried. Most dating samples (dry weight of >3 mg) were directly sent to the Keck Carbon Cycle AMS (Keck-CCAMS) Laboratory at the University of California, Irvine (USA), or the Beta Analytic Testing Laboratory (USA) for ^{14}C measurements. Three dating samples were analyzed at the newly established 0.2 MV MICADAS AMS system housed at Northeast Normal University – the authors' institution (Synal et al., 2007). For these runs, samples were pretreated using the acid–base–acid method and then converted into graphite using an automatic graphitization equipment. Graphitized materials were pressed into cathodes, which were loaded into the MICADAS ion source for ^{14}C measurements, together with standards and blanks to ensure data accuracy. The analytical precision (1σ) of $^{14}C/^{12}C$ was typically better than 2 %.

Plant macrofossils from cores were analyzed at 1 cm intervals for peat sections, except at depths where *Sphagnum* moss macrofossils were scarce, in which case they were analyzed at 2 cm intervals. Briefly, subsamples of 1 cm^3 were immersed in a 2 % NaOH solution for over 6 h, rinsed with distilled water, and then sieved through a 125 µm mesh. The sieved fine debris is unidentifiable organic matter (UOM). This fraction was measured for volume after transfer to a cylinder. The unsieved fraction was examined under a stereomicroscope to identify plant macrofossils. The semi-quantitative Quadrat and Leaf Count Macrofossil Analysis (QLCMA) method was employed (Mauquoy et al., 2010). Average volume percentages of different components of plant remains, including charcoals, were estimated from 20 inspections. Additionally, random individual *Sphagnum* leaves were identified under a compound microscope to the subgenus level (*Sphagnum*, *Acutifolia*, *Cuspidata*, and *Subsecunda*), with their respective percentages calculated.

Sphagnum peat sections of cores were analyzed for *Sphagnum* cellulose carbon and oxygen isotopic compositions, which we use as proxies for local environmental changes, at 1 cm intervals for cores TQ22-C1, TQ22-C2, TQ22-C3, and TQ22-C5 and at 2 cm intervals for cores TQ22-C4 and TQ22-C6. Additional 1–2 cm^3 subsamples were used and first treated like macrofossil subsamples. *Sphagnum* stem tissues (about 20–30 shoots in most cases) were further separated and concentrated after removing their branches under a stereomicroscope. These materials were then extracted for cellulose following the established protocol of the alkaline bleaching method, including treatments with $NaClO_2$–CH_3COOH and NaOH solutions (Loader et al., 1997; Kaislahti Tillman et al., 2010). Homogenized and freeze-dried cellulose materials were weighed and placed into tin capsules for carbon isotope analysis and silver capsules for oxygen isotope analysis, with 0.1–0.3 mg of material used for each. Measurements were carried out at the Northeast Institute of Geography and Agroecology, Chinese Academy of Sciences, using a continuous-flow isotope ratio mass spectrometer (MAT253, Thermo Fisher Scientific, USA) coupled with an elemental analyzer (Flash 2000 HT, Thermo Fisher Scientific, USA). Combustion and pyrolysis modes were set for carbon and oxygen isotope analyses, respectively. By convention, results of isotopic ratios were reported using δ notation (in per mil) referenced to VPDB (Vienna Pee Dee Belemnite) for δ^{13}C and to VSMOW (Vienna Standard Mean Ocean Water) for δ^{18}O. The analytical precision (1σ) was about 0.15 ‰ for δ^{13}C and 0.2 ‰ for δ^{18}O (Xia et al., 2024b).

2.3 Modeling peat accumulation

The results of pre-bomb (before 1950) and post-bomb (after 1950) ^{14}C dates were calibrated into calendar ages based on IntCal20 and Bomb21 NH1 curves, respectively (Reimer et al., 2020; Hua et al., 2022). We utilized a model of peat mass accumulation based on the proportional decay concept (Clymo, 1984; Clymo et al., 1998) to fit the relationship between near-surface cumulative peat masses and peat ages by combining all ^{14}C-dated horizons with post-bomb ages from six cores. This practice assumes that near-surface peat accumulations in different cores are controlled by very similar rates of mass input (litter production) and output (rapid aerobic decay) and that peat of post-bomb ages is still in the acrotelm (surface "aerobic layer") and has not yet been transferred to the catotelm (deep "anaerobic layer"). Considering this model allowed us to assess the post-bomb chronology and reasonably reject unrealistic calibrated ages (calibration of post-bomb ages would yield a possible age from before 1963 and another possible age from after 1963). Additionally, this model yielded key parameters fundamental to understanding the control of peatland C balance.

The model assumes that for a given mass of fresh OM m_0 (g cm^{-2}) produced annually per unit area, the decay process per unit time follows

$$\frac{\mathrm{d}m}{\mathrm{d}t} = -m\alpha\left(\frac{m}{m_0}\right)^x, \quad (1)$$

where m is mass per unit area (g cm^{-2}), t is time (years), α is the decay coefficient (yr^{-1}), and x is an exponent controlling the recalcitrance effect (Morris et al., 2015). As decay progresses, the actual decay rate, $\alpha(m/m_0)^x$, may either remain constant ($x = 0$) or decrease ($x > 0$) over time, particularly more rapidly with higher x. For a peat column where fresh OM is continually added from the top and decayed OM remains and accumulates over time, the cumulative peat mass (M) can be expressed as the time integral of m:

$$M(t) = \int_0^t m\,\mathrm{d}t = \begin{cases} \frac{m_0(1-e^{-\alpha t})}{\alpha} & \text{if } x = 0, \\ \frac{m_0\left[(1+x\alpha t)^{\frac{x-1}{x}}-1\right]}{(x-1)\alpha} & \text{if } x > 0 \text{ and } x \neq 1, \\ \frac{m_0 \ln(1+\alpha t)}{\alpha} & \text{if } x = 1. \end{cases} \quad (2)$$

Equation (2) is a more general expression of the mass–age relationship compared to several special cases shown in Clymo et al. (1998). It was utilized to fit the cumulative peat mass and age data using the least-squares method, resulting in a potential range of values for m_0, α, and x when combined. The fitting was carried out using an iterative orthogonal sampling technique that takes m_0 and α values from a space of 0–0.2 g cm^{-2} and 0–0.2 yr^{-1} after assigning a particular x value (0–10). The best fit under each x value was accepted only if the coefficient of determination (R^2) was > 0.95. A similar fitting practice has been shown by Charman et al. (2013).

In order to interpret peat-core proxy data as time series, we developed age–depth models for the collected cores using piecewise linear interpolations between dated intervals (Zhang et al., 2018a; Sim et al., 2019; Fewster et al., 2023; Cleary et al., 2024). The way we derived age–depth models is based on the fact that our cores have very rapid accumulation rates of near-surface peat but much slower accumulation rates of deeper peat that cannot be dated in high resolution. This approach contrasts Bayesian modeling, which needs to incorporate smoothness-related prior information.

2.4 Other data analyses

To summarize the pattern of peatland vegetation changes, we performed principal component analysis (PCA) to reduce the dimensionality of the macrofossil data, in which important macrofossil types (mean percentage > 1 %) were selected and percentage data were log-transformed.

To quantify changes in peatland C capacity, we calculated long-term apparent C accumulation rates (aCARs; alternatively, "LORCA") for entire peat-core columns, where the C content for OM is based on the mean value (49.7 %) derived from our specific C concentration measurements. These aCAR values represent the net rates of C sequestration during the peat accumulation history and were compared with available net ecosystem C balance (NECB) data derived from contemporary eddy covariance measurements combined with other observations (Sun et al., 2024). We did not present depth-specific aCAR data as time series due to the well-recognized artifact of an increasing trend from old to young peat (Young et al., 2019, 2021).

3 Results

3.1 Peat properties

Peat property data are presented in Fig. 2. Among all subsamples of six cores, the OM content varies from 2.1 % to 100 % and the AFBD varies from 0.014 to 0.311 g cm^{-3}. The OM content profiles show lower values at increasing depth and clearly distinguish the transition from mineral substrate to peat in four cores, which is defined based on the threshold of 30 % OM content (Table 1). The AFBD profiles generally show higher values in sedge peat sections than in young *Sphagnum* peat and old mineral substrate sections (macrofossil data are described in a following subsection). The mean OM content is 92.2 %, 73.4 %, and 7.9 % and the mean AFBD is 0.044, 0.150, and 0.090 g cm^{-3} for *Sphagnum* peat, sedge peat, and mineral substrate, respectively. Among these values, it is noted that the *Sphagnum* peat AFBD is very low and the sedge peat AFBD is very high at our site, compared to the northern peatland database (Loisel et al., 2014).

Among all subsamples of six cores, the C/N ratio (mass ratio) of bulk peat varies from 16 to 77. The C/N ratio profiles show maximum values at shallow depths and much lower values in deeper sections. The stratigraphical transitions into very low C/N ratios with greater depths are related to abrupt changes in botanical composition from *Sphagnum* peat to sedge peat in each core. The mean C/N ratio is 49 for *Sphagnum* peat and 23 for sedge peat. Both values are low compared to the northern peatland database (Loisel et al., 2014).

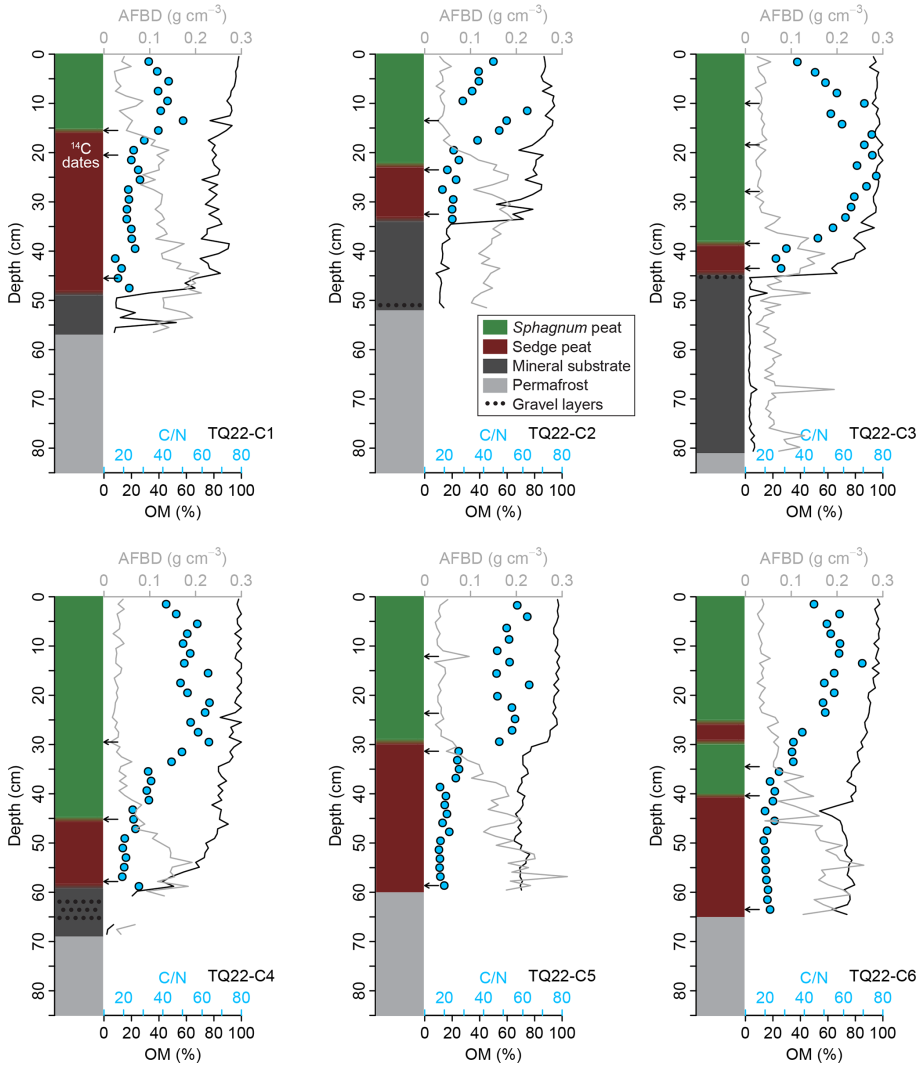

Figure 2. Lithology information and peat properties (organic matter content, ash-free bulk density, C/N ratio) of six cores. Arrows indicate the ^{14}C-dated horizons.

3.2 Radiocarbon dating

Radiocarbon dates and other relevant information are listed in Table 2. We obtained many post-bomb dates, even at > 40 cm depth, pointing to very rapid accumulation rates of near-surface peat. The basal ages in median values are 610, 660, 75, and 600 cal. yr BP (equivalent to 1340, 1290, 1875, and 1350 CE) from cores TQ22-C1, TQ22-C2, TQ22-C3, and TQ22-C4, respectively (Fig. 1c). The bottom of available peat in core TQ22-C6 has the oldest date, at a median age of 2850 cal. yr BP.

3.3 Modeled peat accumulation

Figure 3a shows the biplot between cumulative peat masses and calibrated ages of post-bomb dates. By considering the stratigraphic order and the expected concave pattern of the mass–age relationship, we determined, for each post-bomb date, which of the two calibrated ages should be rejected, and then we can accept the other one as the most likely age for that dating horizon. However, we cannot definitively determine the correct ages for two post-bomb dates: 20–21 cm of TQ22-C1 and 34–35 cm of TQ22-C6. For these dates, calibration yielded two ages that are close to each other, making it difficult to determine which is more reasonable (Fig. 3a and Table 2). We accepted their older calibrated ages due to them being closer to other dates with similar cumulative peat masses.

Combining all these accepted calibrated post-bomb ages, we fitted the mass–age relationship using the general expression of peat decomposition model (Eq. 2) and found that the fitted curves can be robust for a wide range of recalcitrance values up to $x = 1.6$ (Fig. 3a), in which stronger recalcitrance requires higher rates of production and decomposi-

Table 2. Summary of radiocarbon data from Tuqiang peatland.

Core ID and dated depth (cm)	Lab number	Dated material	"Fraction Modern" ($F^{14}C \pm 1\sigma$) for post-bomb dates or ^{14}C *age* (^{14}C *years BP* $\pm 1\sigma$) for pre-bomb dates	Two possible ages (CE) for post-bomb dates or *calibrated age range* (*cal. years BP, 2σ*) for pre-bomb dates
TQ22-C1				
15–16	64306.1.1[a]	*Sphagnum* stems/leaves	1.1102 ± 0.0012	1958, 1995[e]
20–21	UCIAMS-281034[b]	*Sphagnum* stems/leaves	1.4707 ± 0.0022	1962–1963[e], 1972–1973
45–46	UCIAMS-286228	Shrub/herb leaves	*605 ± 15*	*646–585*, *567–551*
46–47	UCIAMS-281035	Shrub/herb leaves	1.0961 ± 0.0029[d]	1957–1958, 1998–2001
TQ22-C2				
13–14	UCIAMS-281036	*Sphagnum* stems/leaves	1.0229 ± 0.0015	1955, 2014–2016[e]
23–24	64307.1.1	Shrub/herb parts and *Sphagnum* stems/leaves	1.0088 ± 0.0011	1954–1955[e], 2018
32–33	UCIAMS-281037	Shrub/herb leaves	*710 ± 70*	*770–762*, *741–545*
TQ22-C3				
9–10	UCIAMS-286229	*Sphagnum* stems/leaves	1.0232 ± 0.0017	1955, 2014–2016[e]
17–18	UCIAMS-281038	*Sphagnum* stems/leaves	1.0450 ± 0.0015	1956, 2010–2011[e]
26–27	UCIAMS-286230	*Sphagnum* stems/leaves	1.0869 ± 0.0018	1957, 2000–2002[e]
36–37	UCIAMS-281039	*Sphagnum* stems/leaves	1.1117 ± 0.0017	1958[e], 1995–1997
43–44	UCIAMS-286231	*Sphagnum* stems/leaves	*25 ± 15*	*245–230*, *135–116*, *60–42*
TQ22-C4				
29–30	UCIAMS-281042	*Sphagnum* stems/leaves	1.0546 ± 0.0018	1956–1957, 2007–2009[e]
45–46	64308.1.1	*Sphagnum* stems/leaves	1.0815 ± 0.0011	1957[e], 2001–2003
58–59	UCIAMS-286232	Shrub/herb leaves	*430 ± 15*	*513–480*
TQ22-C5				
10–11	UCIAMS-286233	*Sphagnum* stems/leaves	1.0285 ± 0.0017	1955–1956, 2012–2014[e]
20–21	UCIAMS-286234	*Sphagnum* stems/leaves	1.0523 ± 0.0018	1956, 2007–2010[e]
27–28	UCIAMS-281043	*Sphagnum* stems/leaves	1.1005 ± 0.0016	1957–1958, 1997–2000[e]
57–58	UCIAMS-281044	Shrub/herb leaves	*650 ± 20*	*663–628*, *594–558*
TQ22-C6				
34–35	UCIAMS-281045	*Sphagnum* stems/leaves	1.3567 ± 0.0020	1962[e], 1975–1976
40–41	Beta-717285[c]	*Sphagnum* stems/leaves	*110 ± 30*	*269–212*, *196–189*, *149–12*
63–64	UCIAMS-281046	Shrub/herb leaves	*2760 ± 15*	*2919–2906*, *2881–2783*

[a] Lab number in such a format means that the sample was analyzed at Northeast Normal University, China. [b] Lab number with "UCIAMS": analyzed at the Keck-CCAMS Laboratory at the University of California, Irvine, USA. [c] Lab number with "Beta": analyzed at the Beta Analytic Testing Laboratory, USA. [d] Rejected outlier date. [e] Selected age based on the stratigraphic order or the mass–age relationship.

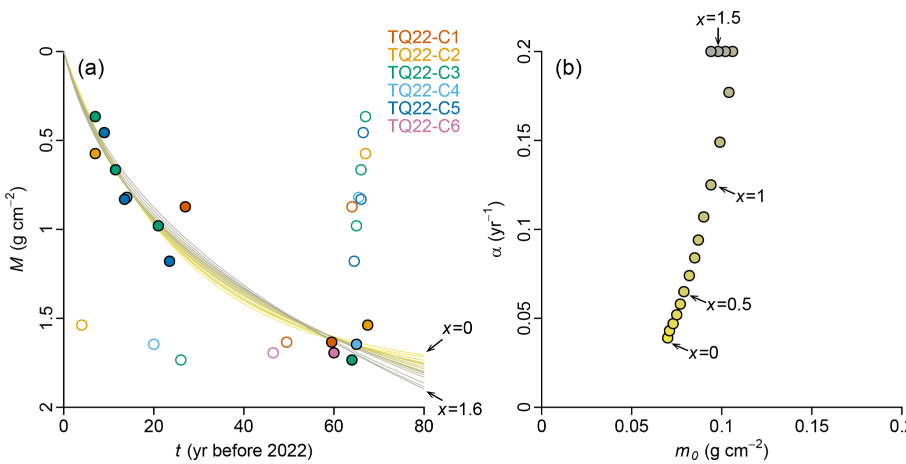

Figure 3. Results of near-surface peat accumulation modeling. **(a)** The relationship between cumulative peat mass (M) and time (t) derived by combining all post-bomb dates of six cores. Rejected ages after post-bomb calibration are shown as open circles. Accepted ages (closed circles) were fitted using the general expression of Clymo's model, with fitted curves plotted in different colors for different assumptions of recalcitrant effects (x). **(b)** The fitted values of annual production m_0 and decay coefficient α under different x values.

tion (Fig. 3b). The choice of $x = 0.8$ (assuming an intermediate recalcitrant effect) produced the highest fit ($R^2 = 0.962$), with $m_0 = 0.087\,g\,cm^{-2}$ and $\alpha = 0.094\,yr^{-1}$. Assuming no recalcitrant effect would yield $m_0 = 0.07\,g\,cm^{-2}$ and $\alpha = 0.039\,yr^{-1}$ ($R^2 = 0.959$), both of which are higher than reported values from the acrotelm of other northern peatlands (Yu et al., 2001; Loisel and Yu, 2013).

3.4 Plant macrofossil records of peatland vegetation changes

Full plant macrofossil diagrams are presented in Figs. A1–A6. Macrofossil analysis reveals transitions from lower sedge (Cyperaceae) peat to upper *Sphagnum* peat in all cores, although cores TQ22-C1 and TQ22-C6 exhibit somewhat fluctuating abundances of Cyperaceae and *Sphagnum* macrofossils across the transition. We define the onset of *Sphagnum* peat over sedge peat in each core as the greatest depth where *Sphagnum* macrofossils exceed 40 % abundance (Table 1 and Fig. 2). The chronology of this stratigraphical transition is well constrained in all six cores. The median ages are 1995, 1955, 1958, 1957, 2001, and 1838 CE, respectively.

PCA identifies the statistical relationship among different macrofossil types (Fig. 4a). The first component explains 31.1 % of variance and separates the contrasting environmental preferences between dry-adapted *Sphagnum* mosses (subgenus *Sphagnum* and *Acutifolia*) and wet-favoring herbaceous taxa (Cyperaceae). However, charcoal fragments, which are often interpreted as a drought indicator, are tightly associated with herbaceous taxa. The second component explains 12.1 % of variance and separates non-*Sphagnum* mosses and Ericaceae, likely related to microhabitat conditions or competition for resources. The PC1 score shows a trend of gradual increase since several hundred years ago, followed by an abrupt increase during the recent century related to the onsets of *Sphagnum* peat accumulation (Fig. 4b).

3.5 Apparent peat carbon accumulation rates

The long-term aCARs for six cores show an age-dependent pattern with the highest aCAR ($163.8\,g\,C\,m^{-2}\,yr^{-1}$) found in the youngest core, TQ22-C3, and the lowest aCAR ($10.4\,g\,C\,m^{-2}\,yr^{-1}$) found in the oldest core, TQ22-C6 (Fig. 5). The other four cores are of similar ages (660–500 cal. yr BP) but still have highly variable aCARs (24.3–$51.2\,g\,C\,m^{-2}\,yr^{-1}$), showing within-site heterogeneity in the rate of C sequestration. In comparison, the currently available NECB at the same site (Fig. 5), derived mostly from atmospheric C flux measurements, indicates a further higher rate of C sequestration at about 55 and $74.2\,g\,C\,m^{-2}\,yr^{-1}$ in 2016 and 2017, respectively (Sun et al., 2024), after additionally accounting for the small fluvial C losses of $4.7\,g\,C\,m^{-2}\,yr^{-1}$ (Guo et al., 2018).

3.6 Isotopic records of environmental changes from *Sphagnum* peat sections

Among all cores, *Sphagnum* cellulose $\delta^{13}C$ ($\delta^{13}C_{cell}$) values range from −32.9 ‰ to −27.9 ‰ and cellulose $\delta^{18}O$ ($\delta^{18}O_{cell}$) values range from 14.1 ‰ to 20.2 ‰. We applied a correction for the "Suess effect" using the method by Leuenberger (2007), which removed the effect of changing $\delta^{13}C$ values of atmospheric CO_2 due to fossil fuel combustion in recent centuries. The "Suess effect"-corrected $\delta^{13}C_{cell}$ values range from −31.7 ‰ to −25.9 ‰. Hereafter, $\delta^{13}C_{cell}$ data mentioned in this paper all refer to their corrected values.

The $\delta^{13}C_{cell}$ records show increasing trends with weak fluctuations since *Sphagnum* mosses became the dominant vegetation in three cores: TQ22-C2, TQ22-C3, and TQ22-C5 (Fig. 6b). However, their increasing trends are not synchronous among different cores. Specifically, the $\delta^{13}C_{cell}$ values of TQ22-C3 increase during the period 1960–1990 and remain stable after that, whereas the $\delta^{13}C_{cell}$ values of TQ22-C2 increase during the entire period of 1960–2020. The $\delta^{13}C_{cell}$ values of TQ22-C5 increase after the 2000s. In the other three cores, the $\delta^{13}C_{cell}$ records do not have clear trends but show weak signs of slightly increasing trends in the cores TQ22-C1 during the recent decade and TQ22-C6 since the 1970s (Fig. 6b).

The $\delta^{18}O_{cell}$ records are characterized by large sample-to-sample fluctuations with no clear trends in all cores (Fig. 6c). This temporal pattern is entirely different from that of the $\delta^{13}C_{cell}$ records. However, chronological uncertainties arising from overly simplistic age–depth models preclude determining whether those $\delta^{18}O_{cell}$ spikes are temporally coherent among different cores or correlating $\delta^{18}O_{cell}$ variations with the inter-annual variability in temperature, precipitation, or precipitation $\delta^{18}O$ (Fig. 6a, d).

4 Discussion

4.1 Possible climate-driven peatland initiation and lateral expansion

A previous global data synthesis of peatland basal ages revealed that growing-season warming during the last deglaciation and early Holocene is the primary driver of the initiation of the most northern peatland areas by enhancing plant productivity (Morris et al., 2018). However, that study included only a limited number of sites from Northeast China. For our site, Han et al. (2019) obtained a basal age of 2620 cal. yr BP (interpolated from their dates between mineral materials and peat) from its northern section, based on one peat core (TQ16) collected from a location west of ours (Fig. 1c). This is much older than our new basal ages and can be interpreted as the timing of peatland initiation. In the southern section, the oldest age of peat cores collected in this study is 2850 cal. yr BP, but it is not the age of basal peat

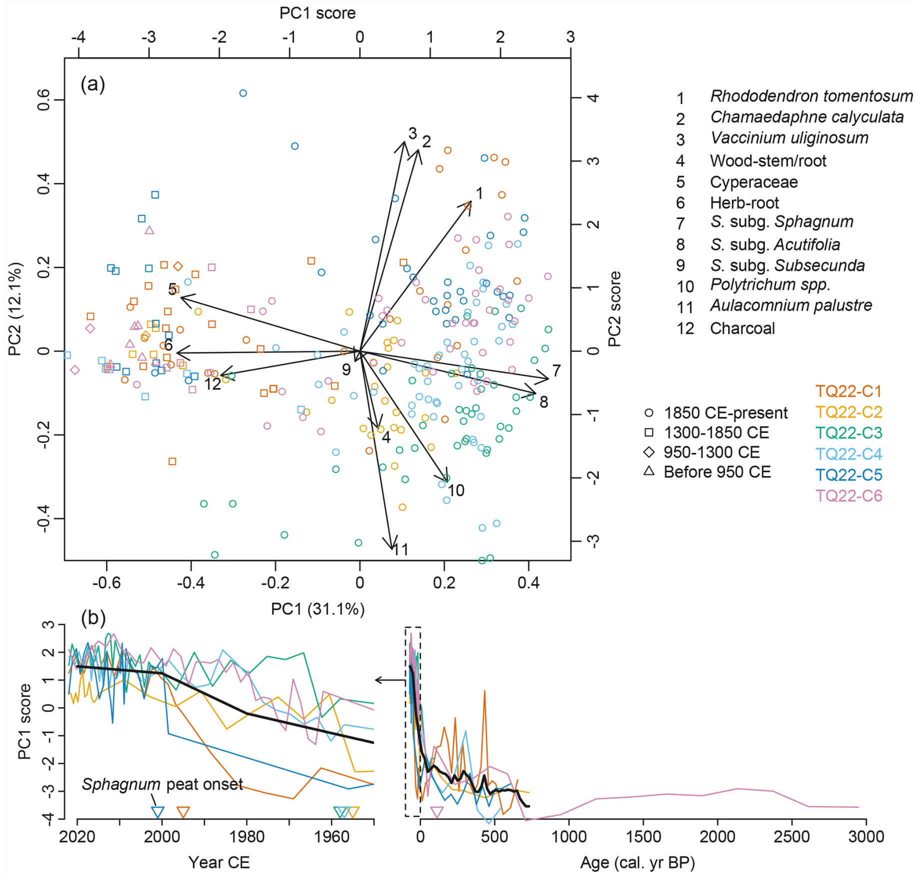

Figure 4. Results of principal component analysis of the macrofossil dataset. **(a)** Component loadings of variables and scores of samples. **(b)** Changes in PC1 score from different cores with a close-up view of the last 70 years. The black line is the 20-year mean of all individual cores. The onsets of *Sphagnum* peat are marked on the *x* axis.

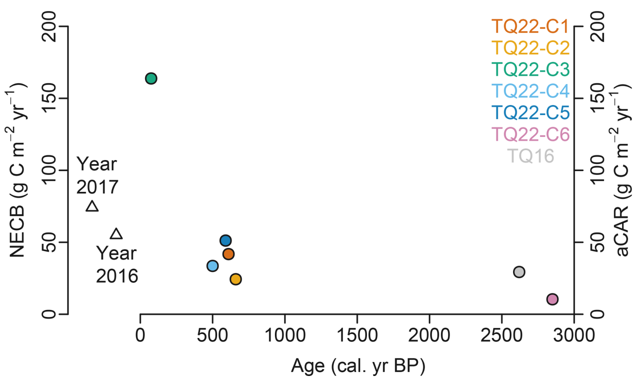

Figure 5. The C sink capacity of Tuqiang peatland. Long-term apparent C accumulation rates (aCARs) of cores collected in this study (TQ22) and a previous study (TQ16) by Han et al. (2019) are plotted against the ages of their basal peat or the bottom of available peat. The annual net ecosystem C balance (NECB) values for the years 2016 and 2017 (Guo et al., 2018; Sun et al., 2024) are plotted on the left side for comparison.

as we did not reach mineral substrate at this coring location (Fig. 1c). Obviously, basal age data from a single site are insufficient for establishing links with large-scale climate forcing. A previous region-wide and comprehensive data synthesis of Northeast China has revealed that the timing of peatland initiation is spatially variable, with more frequent earlier initiations in warmer, lower-latitude locations (Xing et al., 2015). In northern Northeast China including the Greater Hinggan Mountains relevant to this study and the nearby Lesser Hinggan Mountain region, peatland initiation mainly occurred during the late Holocene, i.e., from 4200 cal. yr BP to the present (Fig. 7a; Xing et al., 2015).

The Holocene climate variability has been a subject of debate, particularly regarding (1) whether the Holocene is characterized by long-term cooling as documented by proxy records or long-term warming as simulated by climate models (the Holocene temperature conundrum; Liu et al., 2014b) and (2) whether the early Holocene was wetter than the late Holocene across all monsoon-affected Asian regions as shown in Asian speleothem $\delta^{18}O$ records of monsoon intensity (Wang et al., 2005; Liu et al., 2014a). Fortunately, new

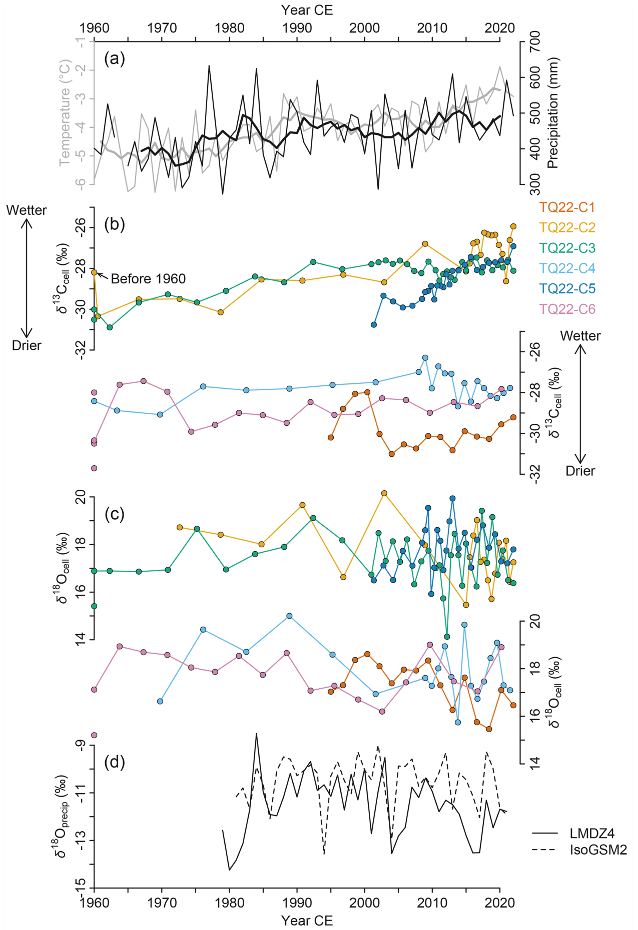

Figure 6. Isotopic records of environmental changes from the period 1960–2022 from high-resolution near-surface peat of six cores. **(a)** Annual temperature and precipitation records from Mohe weather station, located about 24 km from the Tuqiang peatland. **(b)** "Suess effect"-corrected *Sphagnum* $\delta^{13}C_{cell}$ records plotted separately for three cores showing progressively wetter conditions (higher $\delta^{13}C_{cell}$) and three other cores that do not show clear trends. Data from earlier periods (before 1960) are plotted along the left *y* axis. **(c)** Similar to **(b)** but for *Sphagnum* $\delta^{18}O_{cell}$ records. **(d)** Amount-weighted mean growing-season (May–September) precipitation $\delta^{18}O$ for the location of Tuqiang peatland simulated from two nudged isotope-enabled general circulation models, LMDZ4 (Risi et al., 2010) and IsoGSM2 (Yoshimura et al., 2008), the outputs of which are available from the period 1979–2021.

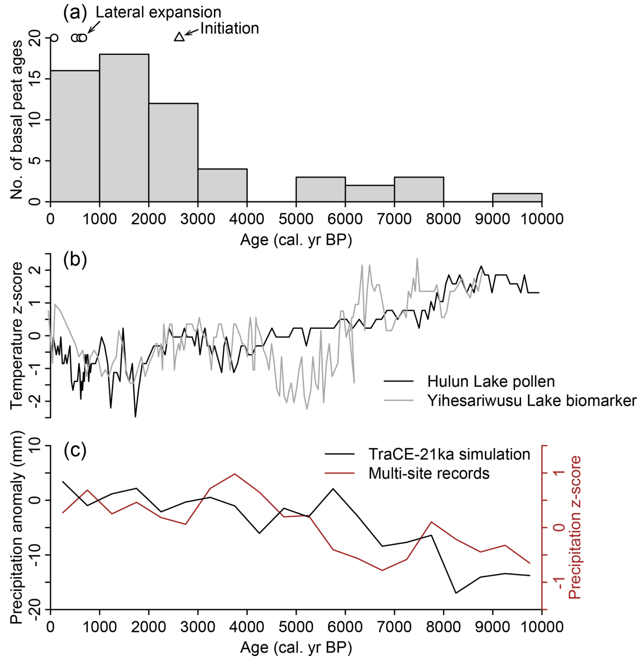

Figure 7. Regional peatland initiation and climate histories during the Holocene. **(a)** Frequency of basal peat ages from the permafrost-affected Greater Hinggan Mountain and Lesser Hinggan Mountain regions, previously compiled by Xing et al. (2015) and Zhang et al. (2020b). Ages of initiation and lateral expansion of Tuqiang peatland are shown as open triangles and dots. **(b)** Temperature changes reconstructed using pollen-based transfer function from Hulun Lake (Wen et al., 2010) and using alkenone biomarkers from Yihesariwusu Lake (Jiang et al., 2024). **(c)** Precipitation changes from a synthesis of multiple proxy records (see Fig. 1b) in northern Northeast China by Zhang et al. (2025), including sites at Huola Basin (Li et al., 2019), Sifangshan Lake (Liu et al., 2017), Tianchi Crater Lake (Zhou et al., 2016; Liu et al., 2019b), and Tanghongling Mire (Yang, 2003), as well as from the model simulation of TraCE-21ka for the same region (Zhang et al., 2025).

studies based on quantitative reconstructions and model–data comparisons provided a timely constraint, showing that the late Holocene – a period of frequent peatland initiations – was characterized by colder and wetter conditions in northern Northeast China compared to the early Holocene (Fig. 7b, c; Jiang et al., 2024; Zhang et al., 2025). This is in remarkable contrast to the global pattern of warming-driven peatland initiations (Yu et al., 2010; Morris et al., 2018).

Previous data syntheses and many site-specific studies showed that after peatland initiation, the peak period of subsequent lateral expansion in northern peatlands occurred during late Holocene cooling (Korhola et al., 2010; Weckström et al., 2010; Ruppel et al., 2013; Quik et al., 2023). These studies suggest that peatland lateral expansion might also be climate-driven, with colder and wetter conditions during these periods facilitating the paludification of surrounding mineral soils (Ruppel et al., 2013). For our site, we obtained three (out of six) peat cores that have young basal peat of similar ages (660–500 cal. yr BP), interpreted as indicating a phase of major peatland lateral expansion. The direction of expansion appears to be from upland toward the river channel (Fig. 1c). The timing is within the Ming–Qing cold period in China (1321–1920), which can be seen as the regional expression of the Little Ice Age (LIA) (Ge et al., 2013; Neukom et al., 2019). A new study using multi-proxy data further suggested that the LIA was characterized by wetter conditions in northern Northeast China (Xia et al., 2024b). Although the lateral expansion of peatlands is poorly documented in our study region, the finding that it occurred at Tuqiang peatland during a climate window of colder and wetter conditions is consistent with the previously identified general pattern in northern peatlands (Ruppel et al., 2013).

Net peat accumulation results from a positive balance between the plant productivity and OM decomposition (Yu et al., 2009). Why are colder and wetter conditions favorable for forming new peatland areas regionally? Superficially, this would suggest that better OM preservation – typically expected under such conditions by slowing down microbial activity – plays a prominent role in initializing and maintaining net peat accumulation. If true, how do we reconcile this finding from the literature that highlights the stronger role of temperature-controlled productivity in shifting the OM balance (Yu et al., 2009; Gallego-Sala et al., 2018; Morris et al., 2018)?

A distinct setting of our study region is that peatlands are primarily found on river floodplains and underlain by permafrost. Early surveys noted a spatial overlap between peat-forming wetlands and permafrost in Northeast China, interpreted as evidence for a symbiotic relationship (Sun, 2000). Geological studies mapping past permafrost boundaries showed that Northeast China was nearly permafrost-free during the warmest period of the Holocene, but the permafrost boundary moved southward by approximately 300 km during the late Holocene and the LIA (Fig. 1b; Jin et al., 2000, 2016). This permafrost history provides a framework for formulating our hypothesis that the transition from seasonally frozen ground to permafrost might be an agent in regional peatland formation. We propose that permafrost aggradation and its possible expansion toward rivers during cooling periods at our site resulted in thinning active layers and reduced water infiltration. These changes likely triggered feedback mechanisms that enhance poorly drained, waterlogged soil conditions locally (Sun, 2000; Ishikawa et al., 2005; O'Donnell et al., 2012), leading to further better OM preservation than by climate cooling and wetting alone and eventually net peat accumulation (Sun, 2000; Treat et al., 2014).

This hypothesis is based on the fact that Tuqiang peatland developed in a floodplain environment, with gravel-/sand-rich sediments observed at the base of cores (Fig. 2). Without permafrost as a physical barrier, rapid and deep drainage through such coarse-grained, highly permeable substrate would prevent soil saturation and also enhance export of dissolved organic C via subsurface flow in a hydrologically connected catchment (Frey and Smith, 2005; Olefeldt and Roulet, 2014; Debolskiy et al., 2021).

Some studies conducted in higher-latitude peatlands have noted that permafrost aggradation may result in the assimilation of undecomposed material into frozen ground, leading to the upward accumulation of labile peat concurrent with syngenetic permafrost (O'Donnell et al., 2012; Treat et al., 2016). In this regime, peat may contain cryostructures (O'Donnell et al., 2012) and often has a very high C/N ratio due to limited C mineralization (Sannel and Kuhry, 2009; Treat et al., 2016; Haugk et al., 2022). However, neither was observed at our site. The C/N ratio of basal and lower peat sections is only about 25 (Fig. 2), showing no sign of freeze protection, compared to > 60 in typical permafrost-affected old peat (Treat et al., 2016). The botanical composition of the peat is dominated by sedges, indicating a prolonged status of wet minerotrophic fen in early peatland history (Figs. 2 and A1–A6). These results provide support for the claim that permafrost aggradation contributed new peat accumulation at our site primarily by maintaining suitable hydrological conditions, rather than by directly freezing the OM.

Together, our analysis links the distinct climate drivers of peatland initiation and lateral expansion with permafrost–hydrology feedback, underscoring the importance of considering surficial geology and cryosphere dynamics in understanding the diverse pathways of peatland formation.

4.2 Vegetation and carbon accumulation dynamics

Plant macrofossils preserved in peatland archives have been used as indicators for long-term ecosystem structure shifts (Hughes and Barber, 2004; Camill et al., 2009; Bauer and Vitt, 2011; Treat et al., 2016). For our site, the macrofossil data show the persistent stability of a wet minerotrophic fen environment dominated by herbaceous vegetation since > 2000 years ago, until recent decades when all cores document a consistent, abrupt transition in vegetation composition toward a present-day dominance of dry-adapted *Sphagnum* mosses (*S.* subg. *Sphagnum* and *S.* subg. *Acutifolia*) and an increased abundance of shrubs as well as dry-adapted *Polytrichum* spp. and *Aulacomnium palustre* (Faber et al., 2016), all indicating a dry ombrotrophic (rainfed) bog environment (Figs. 2 and A1–A6). This transition in core TQ22-C6 appears slightly more complex: *Sphagnum* mosses were present somewhat earlier (median age 1838 CE) and had undergone both abundance fluctuations and species turnovers, but the vegetation composition similar to that in other cores was eventually established in recent decades (Fig. A6). For newly formed peat at core TQ22-C3, a fast sedge–*Polytrichum*/*Aulacomnium*–*Sphagnum* succession can be distinguished (Fig. A3). Principal component analysis of the full macrofossil dataset further reveals that the recent abrupt transition to bog-like vegetation had been preceded by a longer-term slow shift in the same direction since the LIA (Fig. 4b).

While a previous study at the same site has already documented this abrupt transition in vegetation composition, which specifically occurred at about 1895 CE based on the analysis of a single peat core (TQ16; Fig. 1c) (Liu et al., 2024b), our new data from multiple cores make a strong case that this is a site-wide phenomenon of fen–bog transition (FBT) with clear signs of regime-shift behavior, i.e., gradual changes followed by sudden shifts (Scheffer and Carpenter, 2003; Loisel and Yu, 2013; Loisel and Bunsen, 2020).

Instrumental climate data from northern Northeast China indicate a temperature increase by up to 4° C since the end of the nineteenth century (Zhang et al., 2011; Yao et al., 2021). The recent FBT at our site underscores the high sensitivity of ecosystem structures in such young, shallow, and permafrost-underlain peatlands to rapid and large-magnitude climate warming. Loisel and Yu (2013) previously described a conceptual model of "warming-driven FBT" for non-permafrost peatlands to explain how anthropogenic climate warming facilitates *Sphagnum* moss establishment and oligotrophication through surface drying and ecohydrological feedback. For permafrost peatlands, however, we anticipate that the additional permafrost–hydrology feedback further reinforces the processes underlying this model: deepening active layers – the first-stage response to warming-driven permafrost degradation (Swindles et al., 2015; Hugelius et al., 2020) – would further draw down water tables to enhance surface drying. This is supported by our *Sphagnum* $\delta^{13}C_{cell}$ data, which show very low values (corrected values less than −30 ‰) when *Sphagnum* mosses initially replaced herbaceous vegetation in macrofossil records (Fig. 6b), indicating extremely dry conditions when FBT occurred (see the following section, Sect. 4.3, on interpretations of *Sphagnum* $\delta^{13}C_{cell}$ data). Several other studies have documented recent FBT or *Sphagnum* moss expansion in permafrost peatlands elsewhere (Magnan et al., 2018; Taylor et al., 2019; Magnan et al., 2022; Chartrand et al., 2023; Piilo et al., 2023), likely driven by mechanisms similar to those in our record.

There is extensive literature describing the highly dynamic and heterogenous nature of permafrost peatlands with complex ecosystem shifts in response to natural climate variability (Zoltai, 1993; Jones et al., 2013; Gao and Couwenberg, 2015; Treat et al., 2016; Zhang et al., 2018b; Sim et al., 2021; Piilo et al., 2023; Xia et al., 2024a). Specifically, climate-driven permafrost aggradation and degradation can strongly alter surface morphology, forming palsas, peat plateaus, thermokarst collapses, fen–bog complexes, and lakes/ponds, with each following different succession pathways (Olefeldt et al., 2021). However, Tuqiang peatland is a site showing historical stability, along with homogeneity in recent ecosystem shifts and a present-day structure free of relict permafrost landforms (Fig. 1d). We attribute such major differences to the low ice content of regional permafrost compared to the results of previous studies conducted in Europe and North America (Brown et al., 1997; Jin et al., 2016; Olefeldt et al., 2016). Again, our study region is outside the distribution of circum-Arctic thermokarst landscape due to ice-poor conditions (Olefeldt et al., 2016, 2021).

The climate warming, active-layer deepening, and, in particular, the recent transition to the dominance of *Sphagnum* mosses may collectively alter the balance between plant productivity and OM decomposition, with profound consequences for the peatland C sink function (Clymo and Hayward, 1982; van Breemen, 1995; Loisel and Yu, 2013). Some studies have attempted to interpret time series of depth-specific aCARs to understand the temporal shifts in the rate of the C sink (Swindles et al., 2015; Zhang et al., 2018a, 2020a; Sim et al., 2021; Cleary et al., 2024), but direct comparisons between recent and long-term rates can be questioned (Young et al., 2019). Here, we found that the present-day NECB, estimated over 2 monitored years (Guo et al., 2018; Sun et al., 2024), is much higher than the centuries- and millennia-averaged NECB, estimated from long-term aCARs across entire peat-core columns (Fig. 5). This suggests a potential stronger C sink capacity under present conditions compared to the past. However, we caution that the present-day NECB is likely an overestimate due to the short measurement period not accounting for low-frequency disturbances (e.g., wildfire) and the inconsistent methodology (C fluxes are estimated using the concentration gradient method in freezing winter) (Miao et al., 2012b; Sun et al., 2024).

At our site, *Sphagnum* peat accumulation is quite rapid, reaching a thickness of about 40 cm of material over several decades (Fig. 2). Peat accumulation modeling quantifies near-surface peat buildup as being governed by a stable and rapid input of plant litter and stable and rapid proportional decay, with possible recalcitrance in recently formed OM (Fig. 3). Therefore, the present-day stronger C sink is likely related to the persistent surficial peat accumulation from *Sphagnum* litter, which must greatly outweigh any deep C loss caused by deeper active layers and aerobic conditions. Additionally, the generally low C/N ratios of basal and lower peat sections indicate the lack of freeze protection and poor decomposability (Treat et al., 2016; Haugk et al., 2022). Together, our analysis suggests that anthropogenic warming-driven FBT is likely amplified by permafrost–hydrology feedback, with no sign of a reduction in the C sink. In order to understand possible mechanisms for the persistence of the C sink function, we next investigate the pattern of recent environmental changes documented in isotopic ratios of *Sphagnum* macrofossils.

4.3 Ongoing trend toward wetter conditions after the fen–bog transition

Isotopic records from *Sphagnum* macrofossils offer further insights into changes in surface conditions since *Sphagnum* mosses became dominant at our site, providing essential context for understanding ongoing environmental trajectories and their drivers. *Sphagnum* $\delta^{13}C_{cell}$ is a proxy for surface wetness based on the "water film" mechanism, which has been well established through multiple studies (Rice and Giles, 1996; Williams and Flanagan, 1996; Loisel et al., 2009; Xia et al., 2020, 2025). Briefly, higher $\delta^{13}C_{cell}$ values indicate wetter conditions, as a thicker water film on leaf surfaces reduces isotopic fractionation caused by carboxylation (Farquhar et al., 1989). For peatlands like ours relying on precipitation as the primary source of water, *Sphagnum* $\delta^{18}O_{cell}$ is a proxy for precipitation $\delta^{18}O$ (Daley et al., 2010; Granath et al., 2018; Xia et al., 2018), which is controlled by multiple atmospheric drivers such as temperature, precipitation amount or seasonality, and moisture sources (Dansgaard, 1964).

Although the recent FBT phenomenon means that the peatland has become much drier than it used to be, the $\delta^{13}C_{cell}$ records indicate that the peatland has ongoing gradual trends, lacking fluctuations and being asynchronous among different cores, from very dry to wetter conditions after the FBT (Fig. 6b). Such a pattern of moisture changes cannot be simply attributed to a common driver of precipitation, which exhibits large inter-annual variability (Fig. 6a). By contrast, the $\delta^{18}O_{cell}$ records show no clear trend but instead contain large sample-to-sample fluctuations (Fig. 6c), coinciding with the pronounced inter-annual atmospheric variability that may affect precipitation $\delta^{18}O$ (Fig. 6a, d). Therefore, our *Sphagnum* $\delta^{13}C_{cell}$ and $\delta^{18}O_{cell}$ records present two seemingly conflicting phenomena: evidence for the rain-fed nature of *Sphagnum* moss habitats yet no direct effects on their wetness. Here, we interpret these data as indicating that *Sphagnum* wetness is controlled by internal, locally paced surface processes. As described below, we specifically hypothesize that such internal dynamics can be attributed to gradual subsidence from the degradation of ice-poor permafrost or the ecohydrological feedback driven by *Sphagnum* mosses acting as ecosystem engineers.

Previous studies have proposed an empirical stage model predicting that active-layer deepening and surface drying in permafrost peatlands would be succeeded by ground collapse, thermokarst formation, and land surface wetting once thaw progresses into ice-rich layers (Swindles et al., 2015; Hugelius et al., 2020). A newly published global synthesis of peatland water table reconstructions also revealed that those permafrost peatlands showing an ongoing wetting trend had experienced drier "pre-conditions" before the wet shifts (Sim et al., 2021; Zhang et al., 2022). Therefore, the ongoing trend from very dry to wetter conditions over the last several decades documented in our records appears to be an expected outcome for peatlands under warming-driven permafrost degradation. However, field observations at Tuqiang peatland show no sign of peat shrinkage, cracking, or collapse – features that characterize the wetting stage (Fig. 1d). Therefore, unlike the empirical stage model developed for ice-rich peatlands in Europe and North America, we hypothesize that the wetting may be linked to surface subsidence resulting from a combination of gradual thaw and decomposition-induced peat loss, which raised the water table when the effect of active-layer deepening slowed down. For simplicity, we term this general mechanism as surface adjustment–hydrology feedback (Waddington et al., 2015).

Sphagnum mosses are well-known ecosystem engineers that possess multiple plant properties to modify local environmental conditions in ways that favor their success and peat formation (Clymo and Hayward, 1982; van Breemen, 1995; Rydin and Jeglum, 2013). Among these properties, they have an extraordinary water-holding capacity, typically containing several to over 10 times more water than their tissue weight within their hyaline cells and external pore spaces, and they can maintain a capillary fringe to distribute water under various conditions (Clymo and Hayward, 1982; Rydin and Jeglum, 2013). Additionally, *Sphagnum* peat is a poor heat conductor, and as an insulating layer, it may further contribute to slowing down active-layer deepening (van Breemen, 1995; Park et al., 2018). Therefore, we hypothesize that the wetting may also have resulted from plant-mediated ecohydrological feedback (vegetation–hydrology feedback) regulating local moisture dynamics as *Sphagnum* peat gradually built up.

Overall, the isotopic records document internally driven, progressively wetter conditions at Tuqiang peatland over the last several decades, which occurred against a background of long-term drying that had led to the FBT. These two phenomena indicate that anthropogenic climate warming and concurrent permafrost degradation would not lead to complete desiccation (runaway drying scenario; Waddington et al., 2015). Regardless of the actual mechanisms, the peatland demonstrates resilience in mitigating drying. Alongside warming-induced increases in plant productivity (Gallego-Sala et al., 2018), the input of recalcitrant and fire-resistant *Sphagnum* litter (Loisel and Yu, 2013), and increased acidity inhibiting microbial activity (van Breemen, 1995), surface wetting may contribute to maintaining or even enhancing the C sink and might be related to the high NECB observed in atmospheric C flux measurements (Fig. 5).

5 Synthesis and conclusions

Through a detailed multi-core and multi-proxy anatomy of a typical ice-poor permafrost peatland in eastern Eurasia, we are able to understand how peatland formation, succession, and surface conditions responded to past climate variability and identify the roles of permafrost dynamics in regulating these responses. We summarize the main findings as a conceptual diagram describing the evolution of young, shallow, and ice-poor permafrost peatlands under climate change and into the future (Fig. 8). The general conclusions and broad implications are as follows:

1. Permafrost aggradation over permeable mineral-rich soils or substrates is a potentially important but overlooked agent in the formation of new peatland areas by maintaining poorly drained, waterlogged conditions. This permafrost–hydrology feedback highlights the need to consider surficial geology and cryosphere dynamics in understanding the genesis of global peatlands.

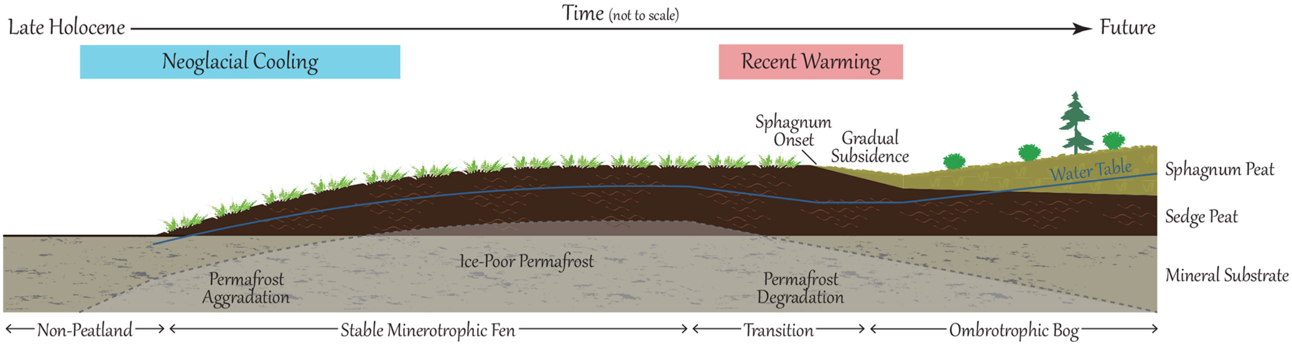

Figure 8. A conceptual diagram for the evolution of young, shallow, and ice-poor permafrost peatlands under climate change based on findings of this study.

2. Ice-poor permafrost peatlands exhibit weak sensitivity to natural climate variability but clear regime-shift behavior under rapid and large-magnitude anthropogenic climate warming. Unlike ice-rich permafrost peatlands with highly dynamic surface morphology, ice-poor permafrost peatlands are characterized by a high degree of stability and homogeneity. The simple succession without involving thermokarst collapse means that their future greenhouse gas emissions and radiative forcing should be substantially smaller than those predicted by models developed for ice-rich permafrost peatlands (Hugelius et al., 2020).

3. Several internal feedback mechanisms may be involved in maintaining the hydrology and C accumulation of ice-poor permafrost peatlands under ongoing climate change. These behaviors reflect peatlands functioning as complex adaptive systems (Belyea and Baird, 2006).

4. Our analysis combining present-day atmospheric C flux measurements presents empirical evidence that similar ice-poor permafrost peatlands in eastern Eurasia are persistent C sinks. Simple protection measures such as fire prevention programs currently being implemented in northern Northeast China will be effective in preserving these significant terrestrial C stocks in the future.

Appendix A: Macrofossil diagram of peatland cores

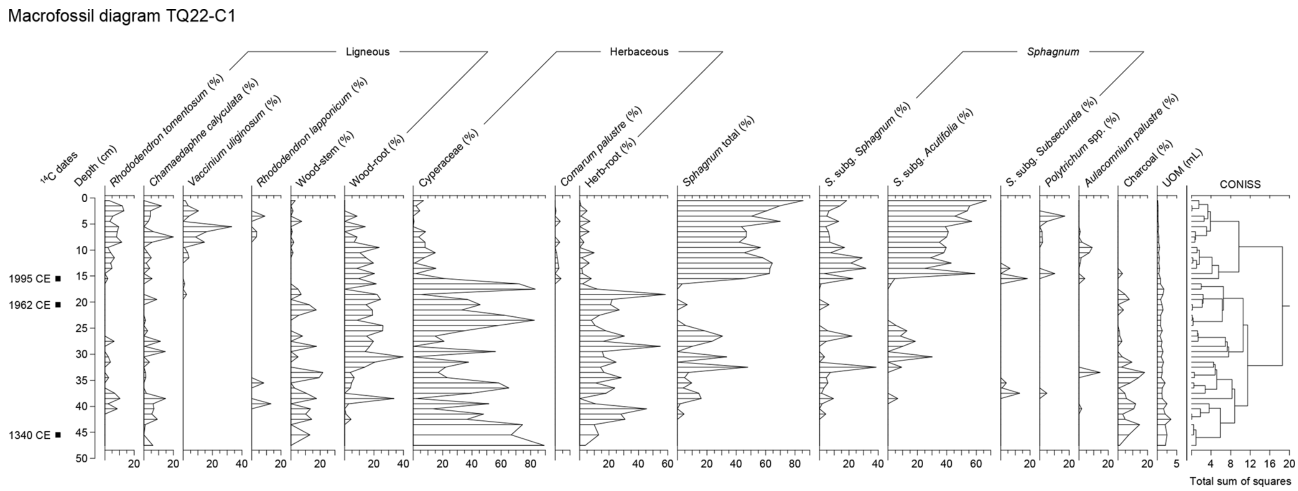

Figure A1. Macrofossil diagram of core TQ22-C1.

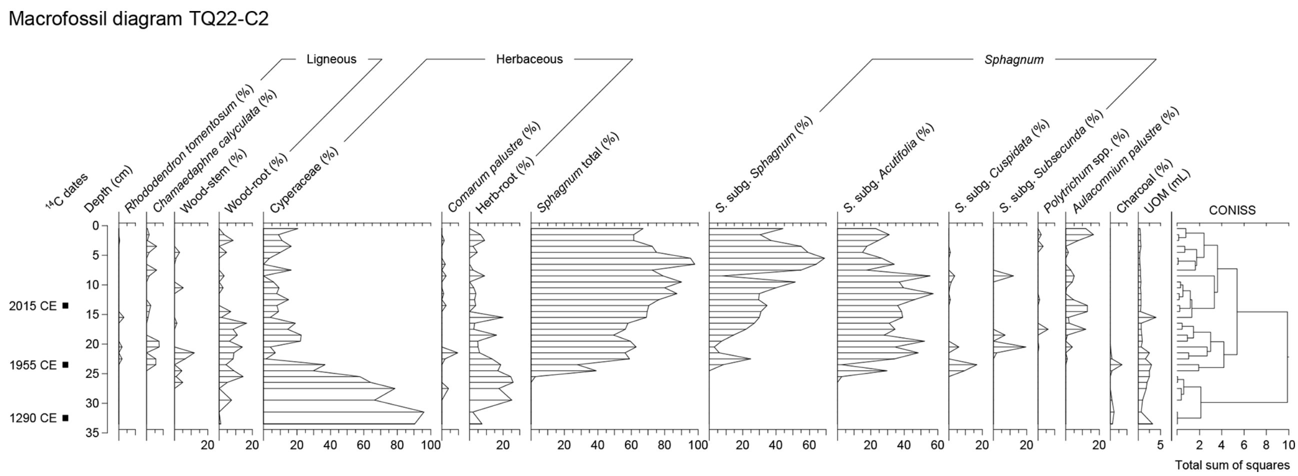

Figure A2. Macrofossil diagram of core TQ22-C2.

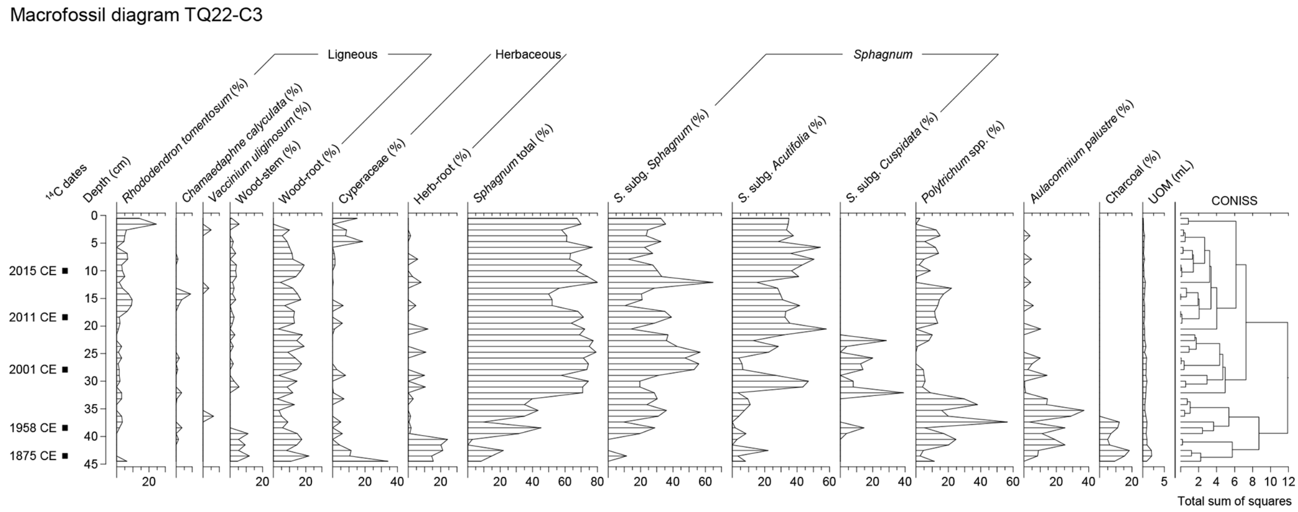

Figure A3. Macrofossil diagram of core TQ22-C3.

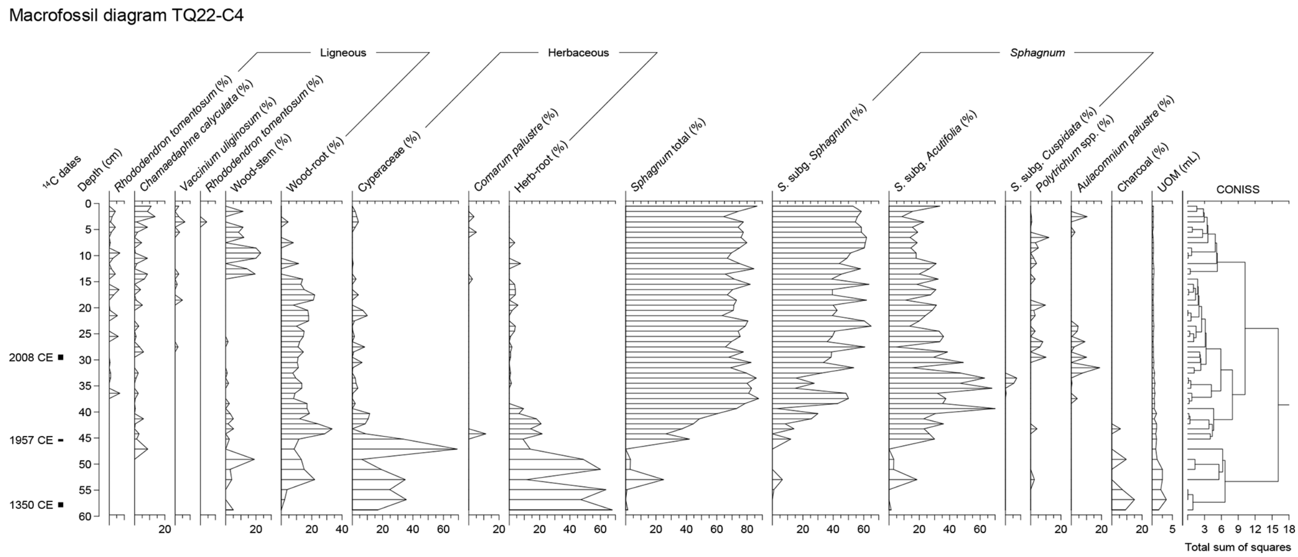

Figure A4. Macrofossil diagram of core TQ22-C4.

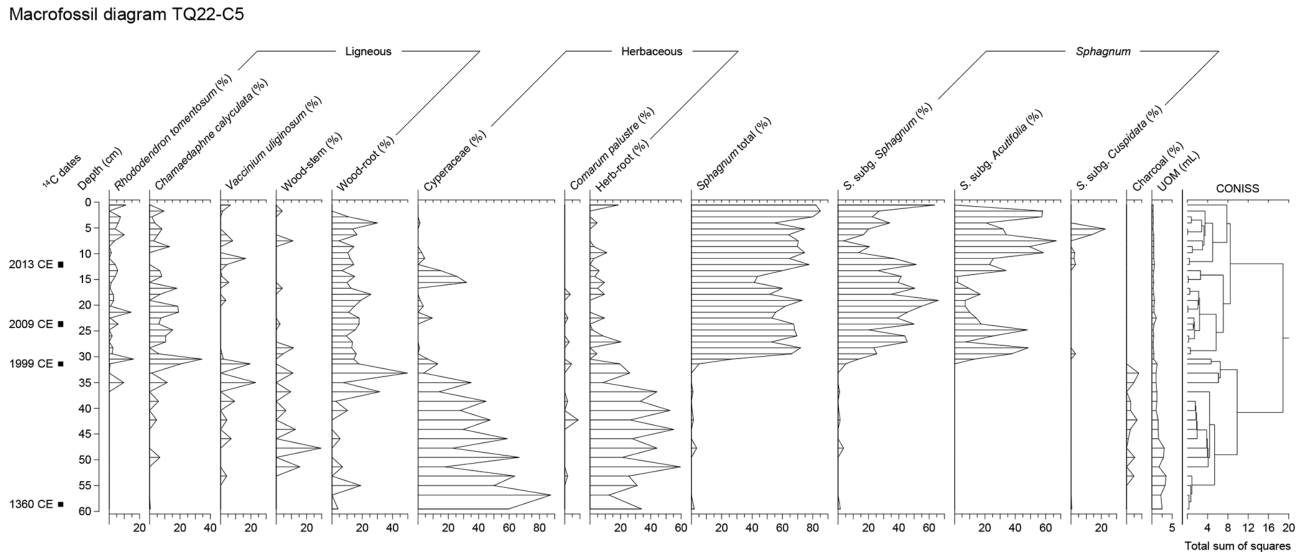

Figure A5. Macrofossil diagram of core TQ22-C5.

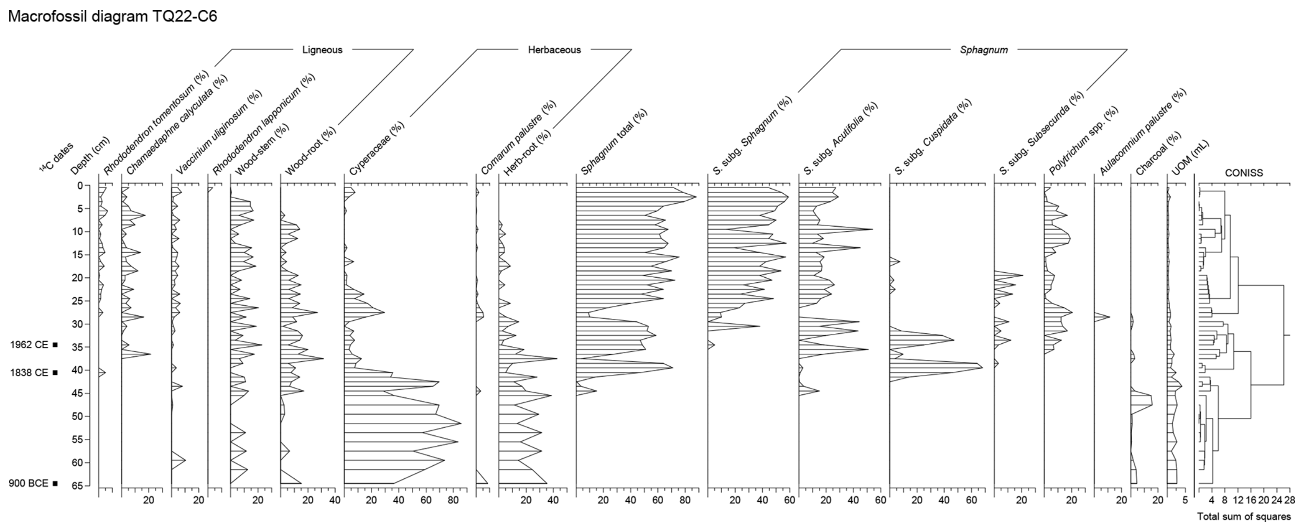

Figure A6. Macrofossil diagram of core TQ22-C6.

Data availability. The data presented in this study are available on request from the corresponding author.

Author contributions. ZY and ZX designed and supervised the study. ZX and FC conducted the fieldwork. FC, MG, and ZX conducted the laboratory work. ZX, FC, and ZY contributed to the data interpretations. ZX and FC wrote the manuscript. ZY edited the manuscript.

Competing interests. The contact author has declared that none of the authors has any competing interests.

Disclaimer. Publisher's note: Copernicus Publications remains neutral with regard to jurisdictional claims made in the text, published maps, institutional affiliations, or any other geographical representation in this paper. While Copernicus Publications makes every effort to include appropriate place names, the final responsibility lies with the authors.

Acknowledgements. We thank Tingwan Yang, Wei Yang, and Shuai Zhang for fieldwork assistance, Yanmin Dong for radiocarbon measurements, Camille Risi for providing LMDZ4 output, Petr Kuneš for editorial guidance, and Sebastian Wetterich and the anonymous reviewer for constructive comments.

Financial support. This research has been supported by the National Natural Science Foundation of China (grant nos. 42330509, 42494822, and 42201167), the Fundamental Research Funds for the Central Universities (grant nos. 2412023YQ006 and 135112004), and the Natural Science Foundation of Jilin Province (grant no. 20230101077JC).

Review statement. This paper was edited by Petr Kuneš and reviewed by Sebastian Wetterich and one anonymous referee.

References

Bao, K., Xing, W., Yu, X., Zhao, H., McLaughlin, N., Lu, X., and Wang, G.: Recent atmospheric dust deposition in an ombrotrophic peat bog in Great Hinggan Mountain, Northeast China, Sci. Total Environ., 431, 33–45, https://doi.org/10.1016/j.scitotenv.2012.05.014, 2012.

Bao, K.-S., Shen, J., Zhang, Y., Wang, J., and Wang, G.-p.: A 200-year record of polycyclic aromatic hydrocarbons contamination in an ombrotrophic peatland in Great Hinggan Mountain, northeast China, J. Mountain Sci., 11, 1085–1096, https://doi.org/10.1007/s11629-014-3167-1, 2014.

Bauer, I. E. and Vitt, D. H.: Peatland dynamics in a complex landscape: Development of a fen-bog complex in the Sporadic Discontinuous Permafrost zone of northern Alberta, Canada, Boreas, 40, 714–726, https://doi.org/10.1111/j.1502-3885.2011.00210.x, 2011.

Belyea, L. R. and Baird, A. J.: Beyond "the limits to peat bog growth": Cross-scale feedback in peatland development, Ecol. Monogr., 76, 299–322, https://doi.org/10.1890/0012-9615(2006)076[0299:BTLTPB]2.0.CO;2, 2006.

Borge, A. F., Westermann, S., Solheim, I., and Etzelmüller, B.: Strong degradation of palsas and peat plateaus in northern Norway during the last 60 years, The Cryosphere, 11, 1–16, https://doi.org/10.5194/tc-11-1-2017, 2017.

Brown, J., Ferrians Jr., O. J., Heginbottom, J. A., and Melnikov, E. S.: Circum-Arctic map of permafrost and ground-ice conditions, Report 45, https://doi.org/10.3133/cp45, 1997.

Camill, P. and Clark, J. S.: Climate change disequilibrium of boreal permafrost peatlands caused by local processes, Am. Nat., 151, 207–222, https://doi.org/10.1086/286112, 1998.

Camill, P., Barry, A., Williams, E., Andreassi, C., Limmer, J., and Solick, D.: Climate-vegetation-fire interactions and their impact on long-term carbon dynamics in a boreal peatland landscape in northern Manitoba, Canada, J. Geophys. Res., 114, G04017, https://doi.org/10.1029/2009JG001071, 2009.

Chambers, F. M., Beilman, D. W., and Yu, Z.: Methods for determining peat humification and for quantifying peat bulk density, organic matter and carbon content for palaeostudies of climate and peatland carbon dynamics, Mires Peat, 7, 7, https://www.mires-and-peat.net/article/128415-methods-for-determining-peat-humification-and-for-quantifying-peat-bulk-density-organic-matter-and-carbon-content-for-palaeostudies-of-climate-and-pe (last access: 1 Ocotber 2025), 2010.

Charman, D. J., Beilman, D. W., Blaauw, M., Booth, R. K., Brewer, S., Chambers, F. M., Christen, J. A., Gallego-Sala, A., Harrison, S. P., Hughes, P. D. M., Jackson, S. T., Korhola, A., Mauquoy, D., Mitchell, F. J. G., Prentice, I. C., van der Linden, M., De Vleeschouwer, F., Yu, Z. C., Alm, J., Bauer, I. E., Corish, Y. M. C., Garneau, M., Hohl, V., Huang, Y., Karofeld, E., Le Roux, G., Loisel, J., Moschen, R., Nichols, J. E., Nieminen, T. M., MacDonald, G. M., Phadtare, N. R., Rausch, N., Sillasoo, Ü., Swindles, G. T., Tuittila, E.-S., Ukonmaanaho, L., Väliranta, M., van Bellen, S., van Geel, B., Vitt, D. H., and Zhao, Y.: Climate-related changes in peatland carbon accumulation during the last millennium, Biogeosciences, 10, 929–944, https://doi.org/10.5194/bg-10-929-2013, 2013.

Chartrand, P. G., Sonnentag, O., Sanderson, N. K., and Garneau, M.: Recent peat and carbon accumulation on changing permafrost landforms along the Mackenzie River valley, Northwest Territories, Canada, Environ. Res. Lett., 18, 095002, https://doi.org/10.1088/1748-9326/ace9ed, 2023.

Cleary, K. G., Xia, Z., and Yu, Z.: The growth and carbon sink of tundra peat patches in Arctic Alaska, J. Geophys. Res.-Biogeo., 129, e2023JG007890, https://doi.org/10.1029/2023JG007890, 2024.

Clymo, R. S.: The limits of peat bog growth, Philos. T. Roy. Soc. B, 303, 368–388, https://doi.org/10.1098/rstb.1984.0002, 1984.

Clymo, R. S. and Hayward, P. M.: The Ecology of *Sphagnum*, in: Bryophyte Ecology, edited by: Smith, A. J. E., Springer Netherlands, Dordrecht, the Netherlands, 229–289, https://doi.org/10.1007/978-94-009-5891-3_8, 1982.

Clymo, R. S., Turunen, J., and Tolonen, K.: Carbon accumulation in peatland, Oikos, 81, 368–388, https://doi.org/10.2307/3547057, 1998.

Cooper, M. D. A., Estop-Aragonés, C., Fisher, J. P., Thierry, A., Garnett, M. H., Charman, D. J., Murton, J. B., Phoenix, G. K., Treharne, R., Kokelj, S. V., Wolfe, S. A., Lewkowicz, A. G., Williams, M., and Hartley, I. P.: Limited contribution of permafrost carbon to methane release from thawing peatlands, Nat. Clim. Change, 7, 507–511, https://doi.org/10.1038/nclimate3328, 2017.

Daley, T. J., Barber, K. E., Street-Perrott, F. A., Loader, N. J., Marshall, J. D., Crowley, S. F., and Fisher, E. H.: Holocene climate variability revealed by oxygen isotope analysis of *Sphagnum* cellulose from Walton Moss, northern England, Quat. Sci. Rev., 29, 1590–1601, https://doi.org/10.1016/j.quascirev.2009.09.017, 2010.

Dansgaard, W.: Stable isotopes in precipitation, Tellus, 16, 436–468, https://doi.org/10.3402/tellusa.v16i4.8993, 1964.

Debolskiy, M. V., Alexeev, V. A., Hock, R., Lammers, R. B., Shiklomanov, A., Schulla, J., Nicolsky, D., Romanovsky, V. E., and Prusevich, A.: Water balance response of permafrost-affected watersheds to changes in air temperatures, Environ. Res. Lett., 16, 084054, https://doi.org/10.1088/1748-9326/ac12f3, 2021.

Errington, R. C., Macdonald, S. E., and Bhatti, J. S.: Rate of permafrost thaw and associated plant community dynamics in peatlands of northwestern Canada, J. Ecol., 112, 1565–1582, https://doi.org/10.1111/1365-2745.14339, 2024.

Estop-Aragonés, C., Cooper, M. D. A., Fisher, J. P., Thierry, A., Garnett, M. H., Charman, D. J., Murton, J. B., Phoenix, G. K., Treharne, R., Sanderson, N. K., Burn, C. R., Kokelj, S. V., Wolfe, S. A., Lewkowicz, A. G., Williams, M., and Hartley, I. P.: Limited release of previously-frozen C and increased new peat formation after thaw in permafrost peatlands, Soil Biol. Biochem., 118, 115–129, https://doi.org/10.1016/j.soilbio.2017.12.010, 2018.

Faber, A. H., Kooijman, A. M., Brinkkemper, O., van der Plicht, J., and van Geel, B.: Palaeoecological reconstructions of vegetation successions in two contrasting former turbaries in the Netherlands and implications for conservation, Rev. Palaeobot. Palynol., 233, 77–92, https://doi.org/10.1016/j.revpalbo.2016.07.007, 2016.

Fan, M., Xin, Z., Ye, L., Song, C., Wang, Y., and Guo, Y.: Changes in soil freeze depth in response to climatic factors in the high-latitude regions of Northeast China, Sustainability, 15, 6661, https://doi.org/10.3390/su15086661, 2023.

Farquhar, G. D., Ehleringer, J. R., and Hubick, K. T.: Carbon isotope discrimination and photosynthesis, Annu. Rev. Plant Physiol. Plant Mol. Biol., 40, 503–537, https://doi.org/10.1146/annurev.pp.40.060189.002443, 1989.

Fewster, R. E., Morris, P. J., Ivanovic, R. F., Swindles, G. T., Peregon, A. M., and Smith, C. J.: Imminent loss of climate space for permafrost peatlands in Europe and Western Siberia, Nat. Clim. Change, 12, 373–379, https://doi.org/10.1038/s41558-022-01296-7, 2022.

Fewster, R. E., Morris, P. J., Swindles, G. T., Ivanovic, R. F., Treat, C. C., and Jones, M. C.: Holocene vegetation dynamics of circum-Arctic permafrost peatlands, Quat. Sci. Rev., 307, 108055, https://doi.org/10.1016/j.quascirev.2023.108055, 2023.

Frey, K. E. and Smith, L. C.: Amplified carbon release from vast West Siberian peatlands by 2100, Geophys. Res. Lett., 32, L09401, https://doi.org/10.1029/2004GL022025, 2005.

Gałka, M., Szal, M., Watson, E. J., Gallego-Sala, A., Amesbury, M. J., Charman, D. J., Roland, T. P., Edward Turner, T., and Swindles, G. T.: Vegetation succession, carbon accumulation and hydrological change in subarctic peatlands, Abisko, northern Sweden, Permafr. Periglac. Process., 28, 589–604, https://doi.org/10.1002/ppp.1945, 2017.

Gallego-Sala, A. V., Charman, D. J., Brewer, S., Page, S. E., Prentice, I. C., Friedlingstein, P., Moreton, S., Amesbury, M. J., Beilman, D. W., Björck, S., Blyakharchuk, T., Bochicchio, C., Booth, R. K., Bunbury, J., Camill, P., Carless, D., Chimner, R. A., Clifford, M., Cressey, E., Courtney-Mustaphi, C., De Vleeschouwer, F., de Jong, R., Fialkiewicz-Koziel, B., Finkelstein, S. A., Garneau, M., Githumbi, E., Hribjlan, J., Holmquist, J., Hughes, P. D. M., Jones, C., Jones, M. C., Karofeld, E., Klein, E. S., Kokfelt, U., Korhola, A., Lacourse, T., Le Roux, G., Lamentowicz, M., Large, D., Lavoie, M., Loisel, J., Mackay, H., MacDonald, G. M., Makila, M., Magnan, G., Marchant, R., Marcisz, K., Martínez Cortizas, A., Massa, C., Mathijssen, P., Mauquoy, D., Mighall, T., Mitchell, F. J. G., Moss, P., Nichols, J., Oksanen, P. O., Orme, L., Packalen, M. S., Robinson, S., Roland, T. P., Sanderson, N. K., Sannel, A. B. K., Silva-Sánchez, N., Steinberg, N., Swindles, G. T., Turner, T. E., Uglow, J., Väliranta, M., van Bellen, S., van der Linden, M., van Geel, B., Wang, G., Yu, Z., Zaragoza-Castells, J., and Zhao, Y.: Latitudinal limits to the predicted increase of the peatland carbon sink with warming, Nat. Clim. Change, 8, 907–913, https://doi.org/10.1038/s41558-018-0271-1, 2018.

Gao, C., He, J., Zhang, Y., Cong, J., Han, D., and Wang, G.: Fire history and climate characteristics during the last millennium of the Great Hinggan Mountains at the monsoon margin in northeastern China, Glob. Planet. Change, 162, 313–320, https://doi.org/10.1016/j.gloplacha.2018.01.021, 2018.

Gao, Y. and Couwenberg, J.: Carbon accumulation in a permafrost polygon peatland: Steady long-term rates in spite of shifts between dry and wet conditions, Global Change Biol., 21, 803–815, https://doi.org/10.1111/gcb.12742, 2015.

Ge, Q., Zheng, J., Hao, Z., and Liu, H.: General characteristics of climate changes during the past 2000 years in China, Sci. China Earth Sci., 56, 321–329, https://doi.org/10.1007/s11430-012-4370-y, 2013.

Gorham, E.: Northern peatlands: Role in the carbon cycle and probable responses to climatic warming, Ecol. Appl., 1, 182–195, https://doi.org/10.2307/1941811, 1991.

Granath, G., Rydin, H., Baltzer, J. L., Bengtsson, F., Boncek, N., Bragazza, L., Bu, Z.-J., Caporn, S. J. M., Dorrepaal, E., Galanina, O., Gałka, M., Ganeva, A., Gillikin, D. P., Goia, I., Goncharova, N., Hájek, M., Haraguchi, A., Harris, L. I., Humphreys, E., Jiroušek, M., Kajukało, K., Karofeld, E., Koronatova, N. G., Kosykh, N. P., Lamentowicz, M., Lapshina, E., Limpens, J., Linkosalmi, M., Ma, J.-Z., Mauritz, M., Munir, T. M., Natali, S. M., Natcheva, R., Noskova, M., Payne, R. J., Pilkington, K., Robinson, S., Robroek, B. J. M., Rochefort, L., Singer, D., Stenøien, H. K., Tuittila, E.-S., Vellak, K., Verheyden, A., Waddington, J. M., and Rice, S. K.: Environmental and taxonomic controls of carbon and oxygen stable isotope composition in *Sphagnum* across broad climatic and geographic ranges, Biogeosciences, 15, 5189–5202, https://doi.org/10.5194/bg-15-5189-2018, 2018.

Guo, Y., Song, C., Tan, W., Wang, X., and Lu, Y.: Hydrological processes and permafrost regulate magnitude, source and chemical characteristics of dissolved organic carbon export in a peatland catchment of northeastern China, Hydrol. Earth Syst. Sci., 22, 1081–1093, https://doi.org/10.5194/hess-22-1081-2018, 2018.

Han, D., Gao, C., Yu, Z., Yu, X., Li, Y., Cong, J., and Wang, G.: Late Holocene vegetation and climate changes in the Great Hinggan Mountains, northeast China, Quat. Int., 532, 138–145, https://doi.org/10.1016/j.quaint.2019.11.017, 2019.

Harris, L. I., Olefeldt, D., Pelletier, N., Blodau, C., Knorr, K.-H., Talbot, J., Heffernan, L., and Turetsky, M.: Permafrost thaw causes large carbon loss in boreal peatlands while changes to peat quality are limited, Global Change Biol., 29, 5720–5735, https://doi.org/10.1111/gcb.16894, 2023.

Haugk, C., Jongejans, L. L., Mangelsdorf, K., Fuchs, M., Ogneva, O., Palmtag, J., Mollenhauer, G., Mann, P. J., Overduin, P. P., Grosse, G., Sanders, T., Tuerena, R. E., Schirrmeister, L., Wetterich, S., Kizyakov, A., Karger, C., and Strauss, J.: Organic matter characteristics of a rapidly eroding permafrost cliff in NE Siberia (Lena Delta, Laptev Sea region), Biogeosciences, 19, 2079–2094, https://doi.org/10.5194/bg-19-2079-2022, 2022.

Heffernan, L., Estop-Aragonés, C., Knorr, K.-H., Talbot, J., and Olefeldt, D.: Long-term impacts of permafrost thaw on carbon storage in peatlands: Deep losses offset by surficial accumulation, J. Geophys. Res.-Biogeo., 125, e2019JG005501, https://doi.org/10.1029/2019JG005501, 2020.

Heffernan, L., Estop-Aragonés, C., Kuhn, M. A., Holger-Knorr, K., and Olefeldt, D.: Changing climatic controls on the greenhouse gas balance of thermokarst bogs during succession after permafrost thaw, Global Change Biol., 30, e17388, https://doi.org/10.1111/gcb.17388, 2024.

Hodgkins, S. B., Tfaily, M. M., McCalley, C. K., Logan, T. A., Crill, P. M., Saleska, S. R., Rich, V. I., and Chanton, J. P.: Changes in peat chemistry associated with permafrost thaw increase greenhouse gas production, P. Natl. Acad. Sci. USA, 111, 5819–5824, https://doi.org/10.1073/pnas.1314641111, 2014.

Hua, Q., Turnbull, J. C., Santos, G. M., Rakowski, A. Z., Ancapichún, S., De Pol-Holz, R., Hammer, S., Lehman, S. J., Levin, I., Miller, J. B., Palmer, J. G., and Turney, C. S. M.: Atmospheric radiocarbon for the period 1950–2019, Radiocarbon, 64, 723–745, https://doi.org/10.1017/RDC.2021.95, 2022.

Hugelius, G., Loisel, J., Chadburn, S., Jackson, R. B., Jones, M., MacDonald, G., Marushchak, M., Olefeldt, D., Packalen, M., Siewert, M. B., Treat, C., Turetsky, M., Voigt, C., and Yu, Z.: Large stocks of peatland carbon and nitrogen are vulnerable to permafrost thaw, P. Natl. Acad. Sci. USA, 117, 20438–20446, https://doi.org/10.1073/pnas.1916387117, 2020.

Hughes, P. D. M. and Barber, K. E.: Contrasting pathways to ombrotrophy in three raised bogs from Ireland and Cumbria, England, Holocene, 14, 65–77, https://doi.org/10.1191/0959683604hl690rp, 2004.

Hunt, S., Yu, Z., and Jones, M.: Lateglacial and Holocene climate, disturbance and permafrost peatland dynamics on the Seward Peninsula, western Alaska, Quat. Sci. Rev., 63, 42–58, https://doi.org/10.1016/j.quascirev.2012.11.019, 2013.

Ishikawa, M., Sharkhuu, N., Zhang, Y., Kadota, T., and Ohata, T.: Ground thermal and moisture conditions at the southern boundary of discontinuous permafrost, Mongolia, Permafr. Periglac. Process., 16, 209–216, https://doi.org/10.1002/ppp.483, 2005.

Jiang, J., Meng, B., Wang, H., Liu, H., Song, M., He, Y., Zhao, C., Cheng, J., Chu, G., Krivonogov, S., Liu, W., and Liu, Z.: Spatial patterns of Holocene temperature changes over mid-latitude Eurasia, Nat. Commun., 15, 1507, https://doi.org/10.1038/s41467-024-45883-y, 2024.

Jin, H.-J., Chang, X.-L., Luo, D.-L., He, R.-X., Lü, L.-Z., Yang, S.-Z., Guo, D.-X., Chen, X.-M., and Harris, S. A.: Evolution of permafrost in Northeast China since the Late Pleistocene, Sciences in Cold and Arid Regions, 8, 269–296, 2016.

Jin, H., Li, S., Cheng, G., Shaoling, W., and Li, X.: Permafrost and climatic change in China, Glob. Planet. Change, 26, 387–404, https://doi.org/10.1016/S0921-8181(00)00051-5, 2000.

Jones, M. C., Booth, R. K., Yu, Z., and Ferry, P.: A 2200-year record of permafrost dynamics and carbon cycling in a collapse-scar bog, interior Alaska, Ecosystems, 16, 1–19, https://doi.org/10.1007/s10021-012-9592-5, 2013.

Jones, M. C., Harden, J., O'Donnell, J., Manies, K., Jorgenson, T., Treat, C., and Ewing, S.: Rapid carbon loss and slow recovery following permafrost thaw in boreal peatlands, Global Change Biol., 23, 1109–1127, https://doi.org/10.1111/gcb.13403, 2017.

Kaislahti Tillman, P., Holzkämper, S., Kuhry, P., Sannel, A. B. K., Loader, N. J., and Robertson, I.: Stable carbon and oxygen isotopes in *Sphagnum fuscum* peat from subarctic Canada: Implications for palaeoclimate studies, Chem. Geol., 270, 216–226, https://doi.org/10.1016/j.chemgeo.2009.12.001, 2010.

Knoblauch, C., Beer, C., Liebner, S., Grigoriev, M. N., and Pfeiffer, E.-M.: Methane production as key to the greenhouse gas budget of thawing permafrost, Nat. Clim. Change, 8, 309–312, https://doi.org/10.1038/s41558-018-0095-z, 2018.

Korhola, A., Ruppel, M., Seppä, H., Väliranta, M., Virtanen, T., and Weckström, J.: The importance of northern peatland expansion to the late-Holocene rise of atmospheric methane, Quat. Sci. Rev., 29, 611–617, https://doi.org/10.1016/j.quascirev.2009.12.010, 2010.

Leuenberger, M.: To what extent can ice core data contribute to the understanding of plant ecological developments of the past?, in: Stable Isotopes as Indicators of Ecological Change, edited by: Dawson, T. E., and Siegwolf, R. T. W., Elsevier, 211–233, https://doi.org/10.1016/S1936-7961(07)01014-7, 2007.

Li, X., Zhao, C., and Zhou, X.: Vegetation pattern of Northeast China during the special periods since the Last Glacial Maximum, Sci. China Earth Sci., 62, 1224–1240, https://doi.org/10.1007/s11430-018-9347-3, 2019.

Li, X., Jin, H., Sun, L., Wang, H., Huang, Y., He, R., Chang, X., Yu, S., and Zang, S.: TTOP-model-based maps of permafrost distribution in Northeast China for 1961–2020, Permafr. Periglac. Process., 33, 425–435, https://doi.org/10.1002/ppp.2157, 2022.

Liu, C., Yue, H., Zhang, W., Yao, Z., Pan, Y., Wang, X., Song, C., Butterbach-Bahl, K., and Dannenmann, M.: Alder expansion stimulates nitrogen oxide (NO_x) emissions from southern Eurasian permafrost peatlands, Global Change Biol., 30, e17368, https://doi.org/10.1111/gcb.17368, 2024a.

Liu, H., Han, D., and Wang, G.: Considering the autogenic processes of the ecosystem to analyze the sensitivity of peatland carbon accumulation to temperature and hydroclimate change, Catena, 236, 107717, https://doi.org/10.1016/j.catena.2023.107717, 2024b.

Liu, H., Yu, Z., Han, D., Gao, C., Yu, X., and Wang, G.: Temperature influence on peatland carbon accumulation over the last century in Northeast China, Clim. Dynam., 53, 2161–2173, https://doi.org/10.1007/s00382-019-04813-1, 2019a.

Liu, J., Liu, Q., Wu, J., Chu, G., and Liu, J.: *N*-alkanes distributions and compound-specific carbon isotope records and their paleoenviromental significance of sediments from Lake Sifangshan in the Great Khingan Mountain, Northeastern China, Journal of Lake Sciences, 29, 498–511, 2017 (in Chinese with an English abstract).

Liu, R., Zhao, L., Wu, X., Cheng, X., Zhang, B., Yang, D., He, J., Wu, S., and Zang, S.: Permafrost peatland initiation and development in Late Holocene of the Northeast China, Ecol. Evol., 15, e71212, https://doi.org/10.1002/ece3.71212, 2025.

Liu, X., Zhan, T., Zhou, X., Wu, H., Li, Q., Zhao, C., Qiao, Y., Jiang, S., Tu, L., Ma, Y., Zhang, J., Jiang, X., Lou, B., Zhang, X., and Zhou, X.: Late onset of the Holocene rainfall maximum in northeastern China inferred from a pollen record from the sediments of Tianchi Crater Lake, Quaternary Res., 92, 133–145, https://doi.org/10.1017/qua.2018.137, 2019b.

Liu, Z., Wen, X., Brady, E. C., Otto-Bliesner, B., Yu, G., Lu, H., Cheng, H., Wang, Y., Zheng, W., Ding, Y., Edwards, R. L., Cheng, J., Liu, W., and Yang, H.: Chinese cave records and the East Asia Summer Monsoon, Quat. Sci. Rev., 83, 115–128, https://doi.org/10.1016/j.quascirev.2013.10.021, 2014a.

Liu, Z., Zhu, J., Rosenthal, Y., Zhang, X., Otto-Bliesner, B. L., Timmermann, A., Smith, R. S., Lohmann, G., Zheng, W., and Elison Timm, O.: The Holocene temperature conundrum, P. Natl. Acad. Sci. USA, 111, E3501–E3505, https://doi.org/10.1073/pnas.1407229111, 2014b.

Loader, N. J., Robertson, I., Barker, A. C., Switsur, V. R., and Waterhouse, J. S.: An improved technique for the batch processing of small wholewood samples to á-cellulose, Chem. Geol., 136, 313–317, https://doi.org/10.1016/S0009-2541(96)00133-7, 1997.

Loisel, J. and Bunsen, M.: Abrupt fen-bog transition across southern Patagonia: Timing, causes, and impacts on carbon sequestration, Front. Ecol. Evol., 8, https://doi.org/10.3389/fevo.2020.00273, 2020.

Loisel, J. and Yu, Z.: Recent acceleration of carbon accumulation in a boreal peatland, south central Alaska, J. Geophys. Res.-Biogeo., 118, 41–53, https://doi.org/10.1029/2012JG001978, 2013.

Loisel, J., Garneau, M., and Hélie, J.-F.: Modern *Sphagnum* δ^{13}C signatures follow a surface moisture gradient in two boreal peat bogs, James Bay lowlands, Québec, J. Quat. Sci., 24, 209–214, https://doi.org/10.1002/jqs.1221, 2009.

Loisel, J., Yu, Z., Beilman, D. W., Camill, P., Alm, J., Amesbury, M. J., Anderson, D., Andersson, S., Bochicchio, C., Barber, K., Belyea, L. R., Bunbury, J., Chambers, F. M., Charman, D. J., De Vleeschouwer, F., Fiałkiewicz-Kozieł, B., Finkelstein, S. A., Gałka, M., Garneau, M., Hammarlund, D., Hinchcliffe, W., Holmquist, J., Hughes, P., Jones, M. C., Klein, E. S., Kokfelt, U., Korhola, A., Kuhry, P., Lamarre, A., Lamentowicz, M., Large, D., Lavoie, M., MacDonald, G., Magnan, G., Mäkilä, M., Mallon, G., Mathijssen, P., Mauquoy, D., McCarroll, J., Moore, T. R., Nichols, J., O'Reilly, B., Oksanen, P., Packalen, M., Peteet, D., Richard, P. J., Robinson, S., Ronkainen, T., Rundgren, M., Sannel, A. B. K., Tarnocai, C., Thom, T., Tuittila, E.-S., Turetsky, M., Väliranta, M., van der Linden, M., van Geel, B., van Bellen, S., Vitt, D., Zhao, Y., and Zhou, W.: A database and synthesis of northern peatland soil properties and Holocene carbon and nitrogen accumulation, Holocene, 24, 1028–1042, https://doi.org/10.1177/0959683614538073, 2014.

Magnan, G., van Bellen, S., Davies, L., Froese, D., Garneau, M., Mullan-Boudreau, G., Zaccone, C., and Shotyk, W.: Impact of the Little Ice Age cooling and 20th century climate change on peatland vegetation dynamics in central and northern Alberta using a multi-proxy approach and high-resolution peat chronologies, Quat. Sci. Rev., 185, 230–243, https://doi.org/10.1016/j.quascirev.2018.01.015, 2018.

Magnan, G., Sanderson, N. K., Piilo, S., Pratte, S., Väliranta, M., van Bellen, S., Zhang, H., and Garneau, M.: Widespread recent ecosystem state shifts in high-latitude peatlands of northeastern Canada and implications for carbon sequestration, Global Change Biol., 28, 1919–1934, https://doi.org/10.1111/gcb.16032, 2022.

Manies, K. L., Jones, M. C., Waldrop, M. P., Leewis, M.-C., Fuller, C., Cornman, R. S., and Hoefke, K.: Influence of permafrost type and site history on losses of permafrost carbon after thaw, J. Geophys. Res.-Biogeo., 126, e2021JG006396, https://doi.org/10.1029/2021JG006396, 2021.

Mauquoy, D., Hughes, P. D. M., and Geel, B. v.: A protocol for plant macrofossil analysis of peat deposits, Mires Peat, 7, 6, https://www.mires-and-peat.net/article/128413-a-protocol-for-plant-macrofossil-analysis-of-peat-deposits (last access: 1 October 2025), 2010.

Miao, Y., Song, C., Sun, L., Wang, X., Meng, H., and Mao, R.: Growing season methane emission from a boreal peatland in the continuous permafrost zone of Northeast China: effects of active layer depth and vegetation, Biogeosciences, 9, 4455–4464, https://doi.org/10.5194/bg-9-4455-2012, 2012a.

Miao, Y., Song, C., Wang, X., Sun, X., Meng, H., and Sun, L.: Greenhouse gas emissions from different wetlands during the snow-covered season in Northeast China, Atmos. Environ., 62, 328–335, https://doi.org/10.1016/j.atmosenv.2012.08.036, 2012b.

Morris, P. J., Baird, A. J., Young, D. M., and Swindles, G. T.: Untangling climate signals from autogenic changes in long-term peatland development, Geophys. Res. Lett., 42, 10788–10797, https://doi.org/10.1002/2015GL066824, 2015.

Morris, P. J., Swindles, G. T., Valdes, P. J., Ivanovic, R. F., Gregoire, L. J., Smith, M. W., Tarasov, L., Haywood, A. M., and Bacon, K. L.: Global peatland initiation driven by regionally asynchronous warming, P. Natl. Acad. Sci. USA, 115, 4851–4856, https://doi.org/10.1073/pnas.1717838115, 2018.

Neukom, R., Steiger, N., Gómez-Navarro, J. J., Wang, J., and Werner, J. P.: No evidence for globally coherent warm and cold periods over the preindustrial Common Era, Nature, 571, 550–554, https://doi.org/10.1038/s41586-019-1401-2, 2019.

Obu, J., Westermann, S., Bartsch, A., Berdnikov, N., Christiansen, H. H., Dashtseren, A., Delaloye, R., Elberling, B., Etzelmüller, B., Kholodov, A., Khomutov, A., Kääb, A., Leibman, M. O., Lewkowicz, A. G., Panda, S. K., Romanovsky, V., Way, R. G., Westergaard-Nielsen, A., Wu, T., Yamkhin, J., and Zou, D.: Northern Hemisphere permafrost map based on TTOP modelling for 2000–2016 at 1 km^2 scale, Earth-Sci. Rev., 193, 299–316, https://doi.org/10.1016/j.earscirev.2019.04.023, 2019.

O'Donnell, J. A., Jorgenson, M. T., Harden, J. W., McGuire, A. D., Kanevskiy, M. Z., and Wickland, K. P.: The effects of permafrost thaw on soil hydrologic, thermal, and carbon dynamics in an Alaskan peatland, Ecosystems, 15, 213–229, https://doi.org/10.1007/s10021-011-9504-0, 2012.

Oksanen, P. O., Kuhry, P., and Alekseeva, R. N.: Holocene development of the Rogovaya River peat plateau, European Russian Arctic, Holocene, 11, 25–40, https://doi.org/10.1191/095968301675477157, 2001.

Olefeldt, D. and Roulet, N. T.: Permafrost conditions in peatlands regulate magnitude, timing, and chemical composition of catchment dissolved organic carbon export, Global Change Biol., 20, 3122–3136, https://doi.org/10.1111/gcb.12607, 2014.

Olefeldt, D., Goswami, S., Grosse, G., Hayes, D., Hugelius, G., Kuhry, P., McGuire, A. D., Romanovsky, V. E., Sannel, A. B. K., Schuur, E. A. G., and Turetsky, M. R.: Circumpolar distribution and carbon storage of thermokarst landscapes, Nat. Commun., 7, 13043, https://doi.org/10.1038/ncomms13043, 2016.

Olefeldt, D., Heffernan, L., Jones, M. C., Sannel, A. B. K., Treat, C. C., and Turetsky, M. R.: Permafrost thaw in northern peatlands: Rapid changes in ecosystem and landscape functions, in: Ecosystem Collapse and Climate Change, edited by: Canadell, J. G., and Jackson, R. B., Springer Nature Switzerland, Cham, Switzerland, 27–67, https://doi.org/10.1007/978-3-030-71330-0_3, 2021.

Park, H., Launiainen, S., Konstantinov, P. Y., Iijima, Y., and Fedorov, A. N.: Modeling the effect of moss cover on soil temperature and carbon fluxes at a tundra site in northeastern Siberia, J. Geophys. Res.-Biogeo., 123, 3028–3044, https://doi.org/10.1029/2018JG004491, 2018.

Payette, S., Delwaide, A., Caccianiga, M., and Beauchemin, M.: Accelerated thawing of subarctic peatland permafrost over the last 50 years, Geophys. Res. Lett., 31, L18208, https://doi.org/10.1029/2004GL020358, 2004.

Piilo, S. R., Väliranta, M. M., Amesbury, M. J., Aquino-López, M. A., Charman, D. J., Gallego-Sala, A., Garneau, M., Koroleva, N., Kärppä, M., Laine, A. M., Sannel, A. B. K., Tuittila, E.-S., and Zhang, H.: Consistent centennial-scale change in European sub-Arctic peatland vegetation toward *Sphagnum* dominance – Implications for carbon sink capacity, Global Change Biol., 29, 1530–1544, https://doi.org/10.1111/gcb.16554, 2023.

Quik, C., van der Velde, Y., Candel, J. H. J., Steinbuch, L., van Beek, R., and Wallinga, J.: Faded landscape: unravelling peat initiation and lateral expansion at one of northwest Europe's largest bog remnants, Biogeosciences, 20, 695–718, https://doi.org/10.5194/bg-20-695-2023, 2023.

Ramm, E., Liu, C., Mueller, C. W., Gschwendtner, S., Yue, H., Wang, X., Bachmann, J., Bohnhoff, J. A., Ostler, U., Schloter, M., Rennenberg, H., and Dannenmann, M.: Alder-induced stimulation of soil gross nitrogen turnover in a permafrost-affected peatland of Northeast China, Soil Biol. Biochem., 172, 108757, https://doi.org/10.1016/j.soilbio.2022.108757, 2022.

Ran, Y., Li, X., Cheng, G., Zhang, T., Wu, Q., Jin, H., and Jin, R.: Distribution of permafrost in China: An overview of existing permafrost maps, Permafr. Periglac. Process., 23, 322–333, https://doi.org/10.1002/ppp.1756, 2012.

Reimer, P. J., Austin, W. E. N., Bard, E., Bayliss, A., Blackwell, P. G., Bronk Ramsey, C., Butzin, M., Cheng, H., Edwards, R. L., Friedrich, M., Grootes, P. M., Guilderson, T. P., Hajdas, I., Heaton, T. J., Hogg, A. G., Hughen, K. A., Kromer, B., Manning, S. W., Muscheler, R., Palmer, J. G., Pearson, C., van der Plicht, J., Reimer, R. W., Richards, D. A., Scott, E. M., Southon, J. R., Turney, C. S. M., Wacker, L., Adolphi, F., Büntgen, U., Capano, M., Fahrni, S. M., Fogtmann-Schulz, A., Friedrich, R., Köhler, P., Kudsk, S., Miyake, F., Olsen, J., Reinig, F., Sakamoto, M., Sookdeo, A., and Talamo, S.: The IntCal20 Northern Hemisphere Radiocarbon Age Calibration Curve (0–55 cal kBP), Radiocarbon, 62, 725–757, https://doi.org/10.1017/RDC.2020.41, 2020.

Rice, S. K. and Giles, L.: The influence of water content and leaf anatomy on carbon isotope discrimination and photosynthesis in *Sphagnum*, Plant Cell Environ., 19, 118–124, https://doi.org/10.1111/j.1365-3040.1996.tb00233.x, 1996.

Risi, C., Bony, S., Vimeux, F., and Jouzel, J.: Water-stable isotopes in the LMDZ4 general circulation model: Model evaluation for present-day and past climates and applications to climatic interpretations of tropical isotopic records, J. Geophys. Res., 115, D12118, https://doi.org/10.1029/2009JD013255, 2010.

Robinson, S. D. and Moore, T. R.: The influence of permafrost and fire upon carbon accumulation in high boreal peatlands, Northwest Territories, Canada, Arct. Antarct. Alp. Res., 32, 155–166, https://doi.org/10.1080/15230430.2000.12003351, 2000.

Ruppel, M., Väliranta, M., Virtanen, T., and Korhola, A.: Postglacial spatiotemporal peatland initiation and lateral expansion dynamics in North America and northern Europe, Holocene, 23, 1596-1606, https://doi.org/10.1177/0959683613499053, 2013.

Rydin, H. and Jeglum, J. K.: The Biology of Peatlands, 2nd edn., Oxford University Press, Oxford, UK, ISBN 9780191810138, https://doi.org/10.1093/acprof:osobl/9780199602995.001.0001, 2013.

Sannel, A. B. K. and Kuhry, P.: Holocene peat growth and decay dynamics in sub-arctic peat plateaus, west-central Canada, Boreas, 38, 13–24, https://doi.org/10.1111/j.1502-3885.2008.00048.x, 2009.

Scheffer, M. and Carpenter, S. R.: Catastrophic regime shifts in ecosystems: linking theory to observation, Trends Ecol. Evol., 18, 648–656, https://doi.org/10.1016/j.tree.2003.09.002, 2003.

Schneider von Deimling, T., Meinshausen, M., Levermann, A., Huber, V., Frieler, K., Lawrence, D. M., and Brovkin, V.: Estimating the near-surface permafrost-carbon feedback on global warming, Biogeosciences, 9, 649–665, https://doi.org/10.5194/bg-9-649-2012, 2012.

Sim, T. G., Swindles, G. T., Morris, P. J., Gałka, M., Mullan, D., and Galloway, J. M.: Pathways for ecological change in Canadian high Arctic wetlands under rapid twentieth century warming, Geophys. Res. Lett., 46, 4726–4737, https://doi.org/10.1029/2019GL082611, 2019.

Sim, T. G., Swindles, G. T., Morris, P. J., Baird, A. J., Cooper, C. L., Gallego-Sala, A. V., Charman, D. J., Roland, T. P., Borken, W., Mullan, D. J., Aquino-López, M. A., and Gałka, M.: Divergent responses of permafrost peatlands to recent climate change, Environ. Res. Lett., 16, 034001, https://doi.org/10.1088/1748-9326/abe00b, 2021.

Smith, L. C., Sheng, Y., and MacDonald, G. M.: A first pan-Arctic assessment of the influence of glaciation, permafrost, topography and peatlands on northern hemisphere lake distribution, Permafr. Periglac. Process., 18, 201–208, https://doi.org/10.1002/ppp.581, 2007.

Sun, G.: Discussion on the symbiotic mechanisms of swamp with permafrost, Journal of Glaciology and Geocryology, 22, 309–316, 2000 (in Chinese with an English abstract).

Sun, L., Song, C., Lafleur, P. M., Wang, X., Tan, W., Du, Y., Qiao, T., and Wang, Y.: Multi-scale temporal variation in CH_4 and CO_2 exchange and associated biophysical controls from two wetlands in Northeast China, Agric. For. Meteorol., 345, 109818, https://doi.org/10.1016/j.agrformet.2023.109818, 2024.

Swindles, G. T., Morris, P. J., Mullan, D., Watson, E. J., Turner, T. E., Roland, T. P., Amesbury, M. J., Kokfelt, U., Schoning, K., Pratte, S., Gallego-Sala, A., Charman, D. J., Sanderson, N., Garneau, M., Carrivick, J. L., Woulds, C., Holden, J., Parry, L., and Galloway, J. M.: The long-term fate of permafrost peatlands under rapid climate warming, Sci. Rep., 5, 17951, https://doi.org/10.1038/srep17951, 2015.

Synal, H.-A., Stocker, M., and Suter, M.: MICADAS: A new compact radiocarbon AMS system, Nucl. Instrum. Methods Phys. Res. Sect. B, 259, 7–13, https://doi.org/10.1016/j.nimb.2007.01.138, 2007.

Taylor, L. S., Swindles, G. T., Morris, P. J., Gałka, M., and Green, S. M.: Evidence for ecosystem state shifts in Alaskan continuous permafrost peatlands in response to recent warming, Quat. Sci. Rev., 207, 134–144, https://doi.org/10.1016/j.quascirev.2019.02.001, 2019.

Treat, C. C., Wollheim, W. M., Varner, R. K., Grandy, A. S., Talbot, J., and Frolking, S.: Temperature and peat type control CO_2 and CH_4 production in Alaskan permafrost peats, Global Change Biol., 20, 2674–2686, https://doi.org/10.1111/gcb.12572, 2014.

Treat, C. C., Jones, M. C., Camill, P., Gallego-Sala, A., Garneau, M., Harden, J. W., Hugelius, G., Klein, E. S., Kokfelt, U., Kuhry, P., Loisel, J., Mathijssen, P. J. H., O'Donnell, J. A., Oksanen, P. O., Ronkainen, T. M., Sannel, A. B. K., Talbot, J., Tarnocai, C., and Väliranta, M.: Effects of permafrost aggradation on peat properties as determined from a pan-Arctic synthesis of plant macrofossils, J. Geophys. Res.-Biogeo., 121, 78–94, https://doi.org/10.1002/2015JG003061, 2016.

Treat, C. C., Kleinen, T., Broothaerts, N., Dalton, A. S., Dommain, R., Douglas, T. A., Drexler, J. Z., Finkelstein, S. A., Grosse, G., Hope, G., Hutchings, J., Jones, M. C., Kuhry, P., Lacourse, T., Lähteenoja, O., Loisel, J., Notebaert, B., Payne, R. J., Peteet, D. M., Sannel, A. B. K., Stelling, J. M., Strauss, J., Swindles, G. T., Talbot, J., Tarnocai, C., Verstraeten, G., Williams, C. J., Xia, Z., Yu, Z., Väliranta, M., Hättestrand, M., Alexanderson, H., and Brovkin, V.: Widespread global peatland establishment and persistence over the last 130,000 y, P. Natl. Acad. Sci. USA, 116, 4822–4827, https://doi.org/10.1073/pnas.1813305116, 2019.

Treat, C. C., Jones, M. C., Alder, J., Sannel, A. B. K., Camill, P., and Frolking, S.: Predicted vulnerability of carbon in permafrost peatlands with future climate change and permafrost thaw in western Canada, J. Geophys. Res.-Biogeo., 126, e2020JG005872, https://doi.org/10.1029/2020JG005872, 2021.

Turetsky, M. R., Wieder, R. K., and Vitt, D. H.: Boreal peatland C fluxes under varying permafrost regimes, Soil Biol. Biochem., 34, 907–912, https://doi.org/10.1016/S0038-0717(02)00022-6, 2002.

Turetsky, M. R., Wieder, R. K., Vitt, D. H., Evans, R. J., and Scott, K. D.: The disappearance of relict permafrost in boreal north America: Effects on peatland carbon storage and fluxes, Global Change Biol., 13, 1922–1934, https://doi.org/10.1111/j.1365-2486.2007.01381.x, 2007.

Turetsky, M. R., Abbott, B. W., Jones, M. C., Anthony, K. W., Olefeldt, D., Schuur, E. A. G., Grosse, G., Kuhry, P., Hugelius, G., Koven, C., Lawrence, D. M., Gibson, C., Sannel, A. B. K., and McGuire, A. D.: Carbon release through abrupt permafrost thaw, Nat. Geosci., 13, 138–143, https://doi.org/10.1038/s41561-019-0526-0, 2020.

van Breemen, N.: How *Sphagnum* bogs down other plants, Trends Ecol. Evol., 10, 270–275, https://doi.org/10.1016/0169-5347(95)90007-1, 1995.

Vitt, D. H., Halsey, L. A., and Zoltai, S. C.: The bog landforms of continental western Canada in relation to climate and permafrost patterns, Arct. Alp. Res., 26, 1–13, https://doi.org/10.1080/00040851.1994.12003032, 1994.

Vitt, D. H., Halsey, L. A., and Zoltai, S. C.: The changing landscape of Canada's western boreal forest: The current dynamics of permafrost, Can. J. For. Res., 30, 283–287, https://doi.org/10.1139/x99-214, 2000.

Voigt, C., Marushchak, M. E., Lamprecht, R. E., Jackowicz-Korczyñski, M., Lindgren, A., Mastepanov, M., Granlund, L., Christensen, T. R., Tahvanainen, T., Martikainen, P. J., and Biasi, C.: Increased nitrous oxide emissions from Arctic peatlands after permafrost thaw, P. Natl. Acad. Sci. USA, 114, 6238–6243, https://doi.org/10.1073/pnas.1702902114, 2017.

Voigt, C., Marushchak, M. E., Mastepanov, M., Lamprecht, R. E., Christensen, T. R., Dorodnikov, M., Jackowicz-Korczyñski, M., Lindgren, A., Lohila, A., Nykänen, H., Oinonen, M., Oksanen, T., Palonen, V., Treat, C. C., Martikainen, P. J., and Biasi, C.: Ecosystem carbon response of an Arctic peatland to simulated permafrost thaw, Global Change Biol., 25, 1746–1764, https://doi.org/10.1111/gcb.14574, 2019.

Waddington, J. M., Morris, P. J., Kettridge, N., Granath, G., Thompson, D. K., and Moore, P. A.: Hydrological feedbacks in northern peatlands, Ecohydrol., 8, 113–127, https://doi.org/10.1002/eco.1493, 2015.

Wang, X., Li, X., Hu, Y., Lv, J., Sun, J., Li, Z., and Wu, Z.: Effect of temperature and moisture on soil organic carbon mineralization of predominantly permafrost peatland in the Great Hing'an Mountains, Northeastern China, J. Environ. Sci., 22, 1057–1066, https://doi.org/10.1016/S1001-0742(09)60217-5, 2010.

Wang, X., Song, C., Chen, N., Qiao, T., Wang, S., Jiang, J., and Du, Y.: Gas storage of peat in autumn and early winter in permafrost peatland, Sci. Total Environ., 898, 165548, https://doi.org/10.1016/j.scitotenv.2023.165548, 2023.

Wang, Y., Cheng, H., Edwards, R. L., He, Y., Kong, X., An, Z., Wu, J., Kelly, M. J., Dykoski, C. A., and Li, X.: The Holocene Asian monsoon: Links to solar changes and North Atlantic climate, Science, 308, 854–857, https://doi.org/10.1126/science.1106296, 2005.

Weckström, J., Seppä, H., and Korhola, A.: Climatic influence on peatland formation and lateral expansion in sub-arctic Fennoscandia, Boreas, 39, 761–769, https://doi.org/10.1111/j.1502-3885.2010.00168.x, 2010.

Wen, L., Guo, M., Huang, S., Yu, F., Zhong, C., and Zhou, F.: The response of vegetation to the change of active layer thickness in permafrost region of the north Greater Khingan Mountains, Journal of Glaciology and Geocryology, 43, 1531–1541, 2021 (in Chinese with an English abstract).

Wen, R., Xiao, J., Chang, Z., Zhai, D., Xu, Q., Li, Y., and Itoh, S.: Holocene precipitation and temperature variations in the East Asian monsoonal margin from pollen data from Hulun Lake in northeastern Inner Mongolia, China, Boreas, 39, 262–272, https://doi.org/10.1111/j.1502-3885.2009.00125.x, 2010.

Williams, T. G. and Flanagan, L. B.: Effect of changes in water content on photosynthesis, transpiration and discrimination against $^{13}CO_2$ and $C^{18}O^{16}O$ in *Pleurozium* and *Sphagnum*, Oecologia, 108, 38–46, https://doi.org/10.1007/BF00333212, 1996.

Xia, Y., Yang, Z., Sun, J., Xia, Z., and Yu, Z.: Late-Holocene ecosystem dynamics and climate sensitivity of a permafrost peatland in Northeast China, Quat. Sci. Rev., 324, 108466, https://doi.org/10.1016/j.quascirev.2023.108466, 2024a.

Xia, Z., Yang, W., and Yu, Z.: Major moisture shifts in inland Northeast Asia during the last millennium, Environ. Res. Lett., 19, 124005, https://doi.org/10.1088/1748-9326/ad8763, 2024b.

Xia, Y., Xia, Z., and Yu, Z.: A 1700-year peatland-based hydroclimate record from the Hengduan Mountains in the southeastern Tibetan Plateau reveals changing dynamics of the summer monsoon interface, Quat. Sci. Rev., 366, 109501, https://doi.org/10.1016/j.quascirev.2025.109501, 2025.

Xia, Z., Yu, Z., and Loisel, J.: Centennial-scale dynamics of the Southern Hemisphere Westerly Winds across the Drake Passage over the past two millennia, Geology, 46, 855–858, https://doi.org/10.1130/G40187.1, 2018.

Xia, Z., Zheng, Y., Stelling, J. M., Loisel, J., Huang, Y., and Yu, Z.: Environmental controls on the carbon and water (H and O) isotopes in peatland *Sphagnum* mosses, Geochim. Cosmochim. Ac., 277, 265–284, https://doi.org/10.1016/j.gca.2020.03.034, 2020.

Xing, W., Bao, K., Guo, W., Lu, X., and Wang, G.: Peatland initiation and carbon dynamics in northeast China: Links to Holocene climate variability, Boreas, 44, 575–587, https://doi.org/10.1111/bor.12116, 2015.

Xu, J., Morris, P. J., Liu, J., and Holden, J.: PEATMAP: Refining estimates of global peatland distribution based on a meta-analysis, Catena, 160, 134–140, https://doi.org/10.1016/j.catena.2017.09.010, 2018.

Yang, Y.: Study on formation and development of forest swamp and paleoenvironment change since the Holocene in the east part of the Xiaoxinganling Mountains, Oceanologia et Limnologia Sinica, 34, 74–82, 2003 (in Chinese with an English abstract).

Yao, Y., Huang, Y., Zhao, J., Wang, L., Ran, Y., Liu, W., and Cheng, H.: Permafrost thaw induced abrupt changes in hydrology and carbon cycling in Lake Wudalianchi, northeastern China, Geology, 49, 1117–1121, https://doi.org/10.1130/G48891.1, 2021.

Yoshimura, K., Kanamitsu, M., Noone, D., and Oki, T.: Historical isotope simulation using reanalysis atmospheric data, J. Geophys. Res., 113, D19108, https://doi.org/10.1029/2008JD010074, 2008.

Young, D. M., Baird, A. J., Charman, D. J., Evans, C. D., Gallego-Sala, A. V., Gill, P. J., Hughes, P. D. M., Morris, P. J., and Swindles, G. T.: Misinterpreting carbon accumulation rates in records from near-surface peat, Sci. Rep., 9, 17939, https://doi.org/10.1038/s41598-019-53879-8, 2019.

Young, D. M., Baird, A. J., Gallego-Sala, A. V., and Loisel, J.: A cautionary tale about using the apparent carbon accumulation rate (aCAR) obtained from peat cores, Sci. Rep., 11, 9547, https://doi.org/10.1038/s41598-021-88766-8, 2021.

Yu, X., Song, C., Sun, L., Wang, X., Shi, F., Cui, Q., and Tan, W.: Growing season methane emissions from a permafrost peatland of northeast China: Observations using open-path eddy covariance method, Atmos. Environ., 153, 135–149, https://doi.org/10.1016/j.atmosenv.2017.01.026, 2017.

Yu, Z., Beilman, D. W., and Jones, M. C.: Sensitivity of northern peatland carbon dynamics to Holocene climate change, in: Carbon Cycling in Northern Peatlands (Geophysical Monograph Series), edited by: Baird, A. J., Belyea, L. R., Comas, X., Reeve, A. S., and Slater, L. D., American Geophysical Union, Washington, DC, USA, 55–69, 2009.

Yu, Z., Turetsky, M. R., Campbell, I. D., and Vitt, D. H.: Modelling long-term peatland dynamics. II. Processes and rates as inferred from litter and peat-core data, Ecol. Model., 145, 159–173, https://doi.org/10.1016/S0304-3800(01)00387-8, 2001.

Yu, Z., Loisel, J., Brosseau, D. P., Beilman, D. W., and Hunt, S. J.: Global peatland dynamics since the Last Glacial Maximum, Geophys. Res. Lett., 37, L13402, https://doi.org/10.1029/2010GL043584, 2010.

Yu, Z., Beilman, D. W., Frolking, S., MacDonald, G. M., Roulet, N. T., Camill, P., and Charman, D. J.: Peatlands and their role in the global carbon cycle, Eos. Trans. AGU, 92, 97–98, https://doi.org/10.1029/2011EO120001, 2011.

Yu, Z. C.: Northern peatland carbon stocks and dynamics: a review, Biogeosciences, 9, 4071–4085, https://doi.org/10.5194/bg-9-4071-2012, 2012.

Zhang, F., Cheng, J., Sun, W., Meng, X., Ni, Z., Wang, Y., and Zhang, E.: Mid-late Holocene meridional out-of-phase precipitation patterns in the margin of the East Asian monsoon region revealed by paleoclimate records and simulations, Quat. Sci. Rev., 352, 109211, https://doi.org/10.1016/j.quascirev.2025.109211, 2025.

Zhang, H., Gallego-Sala, A. V., Amesbury, M. J., Charman, D. J., Piilo, S. R., and Väliranta, M. M.: Inconsistent response of Arctic permafrost peatland carbon accumulation to warm climate phases, Global Biogeochem. Cycles, 32, 1605–1620, https://doi.org/10.1029/2018GB005980, 2018a.

Zhang, H., Piilo, S. R., Amesbury, M. J., Charman, D. J., Gallego-Sala, A. V., and Väliranta, M. M.: The role of climate change in regulating Arctic permafrost peatland hydrological and vegetation change over the last millennium, Quat. Sci. Rev., 182, 121–130, https://doi.org/10.1016/j.quascirev.2018.01.003, 2018b.

Zhang, H., Väliranta, M., Piilo, S., Amesbury, M. J., Aquino-López, M. A., Roland, T. P., Salminen-Paatero, S., Paatero, J., Lohila, A., and Tuittila, E.-S.: Decreased carbon accumulation feedback driven by climate-induced drying of two southern boreal bogs over recent centuries, Global Change Biol., 26, 2435–2448, https://doi.org/10.1111/gcb.15005, 2020a.

Zhang, H., Väliranta, M., Swindles, G. T., Aquino-López, M. A., Mullan, D., Tan, N., Amesbury, M., Babeshko, K. V., Bao, K., Bobrov, A., Chernyshov, V., Davies, M. A., Diaconu, A.-C., Feurdean, A., Finkelstein, S. A., Garneau, M., Guo, Z., Jones, M. C., Kay, M., Klein, E. S., Lamentowicz, M., Magnan, G., Marcisz, K., Mazei, N., Mazei, Y., Payne, R., Pelletier, N., Piilo, S. R., Pratte, S., Roland, T., Saldaev, D., Shotyk, W., Sim, T. G., Sloan, T. J., Słowiński, M., Talbot, J., Taylor, L., Tsyganov, A. N., Wetterich, S., Xing, W., and Zhao, Y.: Recent climate change has driven divergent hydrological shifts in high-latitude peatlands, Nat. Commun., 13, 4959, https://doi.org/10.1038/s41467-022-32711-4, 2022.

Zhang, M., Bu, Z., Wang, S., and Jiang, M.: Moisture changes in Northeast China since the last deglaciation: Spatiotemporal out-of-phase patterns and possible forcing mechanisms, Earth-Sci. Rev., 201, 102984, https://doi.org/10.1016/j.earscirev.2019.102984, 2020b.

Zhang, X.-M., Chen, L., Ji, J.-Z., Wang, J., Wang, Y.-B., Guo, W., and Lan, B.-W.: Climate change and its effect in Harbin from 1881 to 2010, Journal of Meteorology and Environment, 27, 13–20, 2011 (in Chinese with an English abstract).

Zhang, Z., Li, M., Wang, J., Yin, Z., Yang, Y., Xun, X., and Wu, Q.: A calculation model for the spatial distribution and reserves of ground ice – A case study of the Northeast China permafrost area, Eng. Geol., 315, 107022, https://doi.org/10.1016/j.enggeo.2023.107022, 2023.

Zhang, Z., Li, M., Wu, Q., Wang, X., Jin, H., Chen, H., Ma, D., and Zhang, Z.: Degradation and local growth of "Xing'an-Baikal" permafrost responding to climate warming and the consequences, Earth-Sci. Rev., 255, 104865, https://doi.org/10.1016/j.earscirev.2024.104865, 2024.

Zhang, Z.-Q., Wu, Q.-B., Hou, M.-T., Tai, B.-W., and An, Y.-K.: Permafrost change in Northeast China in the 1950s–2010s, Adv. Clim. Change Res., 12, 18–28, https://doi.org/10.1016/j.accre.2021.01.006, 2021.

Zhou, X., Sun, L., Zhan, T., Huang, W., Zhou, X., Hao, Q., Wang, Y., He, X., Zhao, C., Zhang, J., Qiao, Y., Ge, J., Yan, P., Yan, Q., Shao, D., Chu, Z., Yang, W., and Smol, J. P.: Time-transgressive onset of the Holocene Optimum in the East Asian monsoon region, Earth Planet. Sc. Lett., 456, 39–46, https://doi.org/10.1016/j.epsl.2016.09.052, 2016.

Zoltai, S. C.: Cyclic development of permafrost in the peatlands of northwestern Alberta, Canada, Arct. Alp. Res., 25, 240–246, https://doi.org/10.1080/00040851.1993.12003011, 1993.

Zoltai, S. C. and Tarnocai, C.: Perennially frozen peatlands in the western Arctic and subarctic of Canada, Can. J. Earth Sci., 12, 28–43, https://doi.org/10.1139/e75-004, 1975.